AD_____

Award Number: W81XWH-05-1-0291

TITLE: A Partnership Training Program in Breast Cancer Research Using Molecular Imaging Techniques

PRINCIPLE INVESTIGATOR: Paul C. Wang, Ph.D.

CONTRACTING ORGANIZATION: Howard University
Washington, DC 20059

REPORT DATE: July 2006

TYPE OF REPORT: Annual

PREPARED FOR: U.S. Army Medical Research and Materiel Command
Fort Detrick, Maryland 21702-5012

REPORT DOCUMENTATION PAGE

Form Approved
OMB No. 0704-0188

1. REPORT DATE	2. REPORT TYPE	3. DATES COVERED
01-07-2006	Annual	1 Jul 2005 – 30 Jun 2006

4. TITLE AND SUBTITLE

A Partnership Training Program in Breast Cancer Research Using Molecular Imaging Techniques

5a. CONTRACT NUMBER

5b. GRANT NUMBER
W81XWH-05-1-0291

5c. PROGRAM ELEMENT NUMBER

6. AUTHOR(S)

Paul C. Wang, Ph.D.

5d. PROJECT NUMBER

5e. TASK NUMBER

5f. WORK UNIT NUMBER

7. PERFORMING ORGANIZATION NAME(S) AND ADDRESS(ES)

Howard University
Washington, DC 20059

8. PERFORMING ORGANIZATION REPORT NUMBER

9. SPONSORING / MONITORING AGENCY NAME(S) AND ADDRESS(ES)
U.S. Army Medical Research and Materiel Command
Fort Detrick, Maryland 21702-5012

10. SPONSOR/MONITOR'S ACRONYM(S)

11. SPONSOR/MONITOR'S REPORT NUMBER(S)

12. DISTRIBUTION / AVAILABILITY STATEMENT
Approved for Public Release; Distribution Unlimited

13. SUPPLEMENTARY NOTES
Original contains colored plates: ALL DTIC reproductions will be in black and white.

14. ABSTRACT
In the first year of this training grant, five faculty members from different departments at the Howard University were trained in molecular imaging with the faculty at the In Vivo Cellular Molecular Imaging Center at the Johns Hopkins University. Two research projects have started and progressed well. A Molecular Imaging Laboratory, a university core facility, has been established. Major optical imaging equipment, Xenogen IVIS 200, was acquired through this funding. The Molecular Imaging Lab is staffed with an imaging scientist, a molecular biologist, a pharmacologic chemist, and a research assistant. The lab has regular bi-weekly group meetings, a journal club, seminars, and workshops. The trainees have attended various seminars and a one-day retreat at JHU. The PI and the partnership leader have been coordinating the training efforts through meetings and emails. One paper is published and another manuscript is under review.

15. SUBJECT TERMS
training, molecular imaging, breast cancer, optical imaging, magnetic resonance imaging

16. SECURITY CLASSIFICATION OF:				18. NUMBER OF PAGES	19a. NAME OF RESPONSIBLE PERSON
					USAMRMC
a. REPORT	b. ABSTRACT	c. THIS PAGE			19b. TELEPHONE NUMBER *(include area code)*
U	U	U	UU	48	

Standard Form 298 (Rev. 8-98)
Prescribed by ANSI Std. Z39.18

Table of Contents

A Partnership Training Program In Breast Cancer Research Using Molecular Imaging Techniques

I. INTRODUCTION

Advances in molecular and cell biology techniques in recent years have had a marked effect on our understanding of the cellular and molecular mechanisms of cancers, including breast cancer. Significant strides have also been made in the development of a noninvasive, high-resolution, in vivo imaging technology such as positron emission tomography (PET), magnetic resonance imaging (MRI), and optical imaging techniques for better imaging of tumors. In vivo molecular imaging, which utilizes these two fronts, opens up an extraordinary opportunity for studying diseases noninvasively, and in many cases, quantitatively at the molecular level (1-4). Molecular imaging is a growing research discipline aimed at developing and testing novel tools, reagents, and methods to image specific molecular pathways in vivo, particularly those that are key targets in disease processes.

The current assessment of breast cancer depends on anatomic and physiological changes of the disease. These changes are a late manifestation of the molecular changes that truly underlie the disease. If imaging of these early molecular changes is possible, it will directly affect patient care by allowing much earlier detection of the disease. Potentially, clinicians may be able to image molecular changes that currently are defined as "predisease states". This will allow intervention at a time when the outcome is most likely to be affected. In addition, by directly imaging the underlying alterations of disease, the effects of therapy may be monitored shortly after therapy has been initiated in contrast to the many months often required today (5).

In this proposed training program, a partnership between Howard University (HU) and the In Vivo Cellular Molecular Imaging Center (ICMIC) at Johns Hopkins University (JHU) will be established to pursue the molecular imaging research of breast cancer. At Howard University, this partnership will involve a multidisciplinary consortium of five departments. The program is composed of two components: a research component and a broad training component. Howard University faculty will obtain training through conducting collaborative research and by participating in a broad based training program. Experts from Johns Hopkins will participate in training by offering laboratory internships, mentoring research efforts, and conducting seminars and workshops. Through this program, a core facility will also be established to support sustainable long-term molecular imaging research at Howard University.

Our goal for this program is to provide faculty trainees at Howard with basic and updated molecular imaging techniques that they can employ while conducting breast cancer research. The program objectives are:

1. Train new researchers in the breast cancer imaging field using molecular imaging techniques.
2. Offer molecular imaging and breast cancer-related lectures, seminars, workshops, and laboratory internships.
3. Conduct two proposed research projects:
    a. Magnetic Resonance (MR) Image Enhancement by Tumor Cell Targeted Immunoliposome Complex Delivered Contrast Agent.
    b. Imaging the Effects of Macrophage Function on Tumor Progression.
4. Establish a molecular imaging core to support long-term sustainable research.
5. Research concept development and submission grants in breast cancer imaging.

II. BODY

This training program consists of two components: a research component and a broad based training component. The research component includes two research projects and the establishment of a molecular imaging core facility at Howard University. A general description and the progress of the each component are listed as follows:

II.1 Research Components: (a) Research Projects (b) Establish a Molecular Imaging Core Facility

(a) Research Projects:

Project 1: MR Image Enhancement by Tumor Cell Targeted Immunoliposome Complex Delivered Contrast Agent

Tumor imaging exploits the differences in physical properties between malignant and normal tissues. These differences are often insufficient for good contrast resolution (5). Imaging techniques that improve tumor detection, localization and evaluation of therapy and prognosis would be highly desirable (6,7). Contrast-enhanced magnetic resonance imaging is one of the best noninvasive methodologies available today in clinical medicine for assessing anatomy and function of tissues (8). High spatial resolution and high soft tissue contrast are desirable features of noninvasive MRI. However, due to intrinsically low sensitivity, high local concentration of contrast agents (CA) is required to generate detectable MR contrast. A large amount of CA has to be used due to the non-specific uptake by tumors and other tissues *in vivo*. In recent years, targeted CA delivery systems have been developing based on the concept that molecular imaging can increase the signal to noise ratio by detecting the difference in 'molecular properties' between cancer and normal tissues (9-11). This should, in theory, allow for detection of smaller tumors. As one strategy, monoclonal antibodies or antibody fragments have been coupled with CA directly or linked with CA through liposome (Lip) carrier. High concentration of antibody-mediated CA such as Gd provides high T1 positive contrast *in vivo*, but insufficient direct linkage of Gd with antibody or the large molecular size of antibody-Lip-Gd particles may limit its use for imaging cell-surface receptors in solid tumors because of inefficient extravasation and very slow diffusion in the interstitial compartment (6, 12,13). Furthermore, antibody immunogenicity, poor stability of the conjugates and potential change of the antibody binding ability due to changes in surface antigens are still problematic for *in vivo* application. A ligand with less toxic, high binding specificity for tumors, relative small size and without immunogenicity is required to target the CA to tumors.

Optical imaging offers several advantages over other imaging techniques. Among these are simplicity of the technique, high sensitivity and absence of ionizing radiation. There is a general increase in the development of techniques for *in vivo* evaluation of gene expression, monitoring of gene delivery and real-time intraoperative visualization of tumor margins and metastatic lesions to improve surgical outcome (14-16). Limited depth of light penetration and lack of tomographic information prevent *in vivo* efficiency of optical imaging. In order to overcome the limitations of various imaging modalities, multimodal probes have been developed for detection using multiple imaging devices (17-19).

Transferrin receptor (TfR) is a cell-surface internalizing receptor responsible for almost all iron sequestration in mammalian cells. Overexpression of TfR is reported on human cancers from various tissues including breast and is of great value in grading tumors and determining

prognosis (20). TfR has been successfully applied as a molecular target to direct therapeutic agents to tumor cells (21). Transferrin (Tf), the TfR ligand, is a monomeric glycoprotein that binds Fe^{3+} atoms for delivery to vertebrate cells through receptor-mediated endocytosis. Fluorescently labeled Tf has greatly aided the investigation of endocytosis *in vitro*. *In vivo* use of the physiological serum protein Tf is less likely to cause adverse reactions. Indeed, Tf has been successfully used in targeted gene therapy (22,23). We hypothesized that near-infrared dye (NIR) labeled Tf (Tf^{NIR}) would be an ideal ligand and would selectively increase the cellular uptake of MRI and optical reporters *in vivo*, resulting in contrast-enhanced MRI and NIR-based optical detection. Herein, we developed a Tf- and Lip-mediated dual molecular probe with both fluorescent and magnetic reporter groups. The Tf^{NIR} was linked on the surface of Lip, whereas the MRI CA (Magnevist) was encapsulated within the Lip. These components conjugated together and formed uniform vesicles with less than 100 nm in diameter. *In vitro* analysis demonstrated that the probe dramatically improved the uptake of CA and NIR dye in culture cells through both receptor- and Lip-mediated endocytosis. *In vivo*, the probe significantly enhanced the magnetic resonance signals from the tumors and was superior to the CA alone for identifying the tumor morphology and infrastructure. Simultaneously a significant preferential accumulation of fluorescent signal by the tumors was clearly detectable in Tf^{NIR}-based optical imaging. Based on these findings, we have published a paper on the J Molecular Imaging (listed in the Reportable Outcomes) and a second manuscript entitled "Dual Probe with Fluorescent and Magnetic Properties for Imaging Solid Tumor Xenografts" (listed in the Appendices) has been submitted for publication.

Project 2: Imaging the Effects of Macrophage Function on Tumor Promotion

In this study, we will use bioluminescent imaging to measure the effects of exposure to activated macrophages (in *in vitro* co-culture) on the metastatic potential of MCF-7 and MDA-MB-231 cells in nude mice. MCF-7 cells are moderately tumorigenic but not metastatic; MDA-MB-231 cells are highly tumorigenic and metastatic in the nude mouse model. One aim of this study is to determine whether paracrine signaling between activated macrophages and non-metastatic breast cancer cells can increase their invasive potential. In addition, we would like to determine whether anti-inflammatory pharmacological agents would inhibit or promote macrophage-induced metastasis. For these studies we are using MCF-7-Luc-F5 and MDA-MB-231 cells carrying a luciferase transgene under the control of a constitutive promoter (CMV). The cells were obtained from Xenogen Corporation. Initial work on the MCF-7-Luc-F5 cells revealed significant differences in the growth patterns of MCF-7-Luc-F5 cells when grown under the conditions recommended by the supplier. When grown in RPMI Medium 1640 supplemented with 10% FBS and 10 μg/ml bovine insulin, sodium pyruvate and non-essential amino acids, the cells showed a pattern of growth characterized by a mixture of multi-layered foci and monolayer growth. This pattern was dramatically different from that shown by parental MCF-7 cells grown in MEM without insulin, non-essential amino acids, sodium pyruvate and phenol red—the preferred medium for growth of MCF-7. Therefore, it was necessary to identify the conditions under which the cells would show a gross morphology and pattern of growth similar to MCF-7 cultured in MEM without insulin, sodium pyruvate, and non-essential amino acid supplementation, while retaining the luciferase construct (as determined by selection in G418-containing medium). Xenogen notes in its product literature that the MCF-7-Luc-F5 cells have a doubling time of 22 hours as compared to 40 hours for the parental MCF-7 cell line. This lower doubling time translates into an intrinsic growth rate that is approximately twice that of MCF-7.

We have adapted MCF-7-Luc-F5 cells to conditions similar to those under which MCF-7 cells are maintained: We now grow MCF-7-Luc-F5 cells in MEM medium (Gibco-BRL), supplemented with 8.0% FBS, L-glutamine, and antibiotics (penicillin/streptomycin), in the absence of recombinant human insulin (bovine insulin is no longer available from the recommended supplier) and phenol red, which has been observed to be estrogenic. We are currently characterizing MCF-7-Luc-F5 cells with respect to inflammation- and metastasis-associated gene expression already demonstrated in our lab for the parental MCF-7 cell line. The same procedures will have to be performed for the transfected MDA-MB-231 cells (Xenogen). It is necessary to establish that the constructs carried by the luciferase-transfected cell lines do not alter their growth or invasiveness.

(b) Establish a Molecular Imaging Core Facility

It is essential for Howard to establish a basic infrastructure that is capable of supporting a sustainable long-term research program in the field of molecular imaging of breast cancer after this training program. This infrastructure is necessary to provide the researchers with tools to perform the proposed researched projects as well as to provide a broader research training experience. The core of the infrastructure is built upon the existing Biomedical NMR Laboratory in the Howard University Cancer Center. The Biomedical NMR Laboratory has two NMR machines capable of small animal imaging. Through this program, we have acquired a bioluminescence instrument (Xenogen IVIS), which enables us to study stromal inflammation and the internalization of contrast agent. This new optical imaging instrument has significantly enhanced the molecular imaging capabilities of the research core at Howard University. This has complement the existing NMR imaging facility at Howard University. The pictures of NMR machines and the Xenogen machine are posted in the Appendices. The core facility also includes other optical instruments such as a fluorescent microscope. The staff of the molecular imaging core includes an imaging scientist, a molecular biologist, a research assistant, and the staff from the Biomedical NMR Laboratory. The molecular imaging core will attract more faculty members into molecular imaging research and will serve as a center to train future minority scientists in this field.

II.2 Broad Based Training Components

The Molecular Imaging Lab has a regular bi-weekly group meetings, journal club, and seminars. In addition, the lab organized three special workshops on MRI and optical imaging instrumentation. There were three special guest seminars on molecular imaging. The trainees have attended various seminars and a one-day retreat at JHU ICMIC. The trainees have been introduced the JHU ICMIC imaging facilities and the small animal holding area. The trainees have an in-depth group meeting with faculty from JHU to exchange ideas and discussing various aspects of the research. The PI and the partnership leader at JHU have been coordinating the training efforts through meetings and emails. Together, we have submitted a paper for publication.

Workshops and Special Guest Seminars:

1. Workshop: Bruker 400 MHz BioSpin system software and hardware training, Dr. Kang Xu, Bruker Companies, Oct 19-21, 2005.
2. Workshop: Practical Training on Xenogen IVIS 200 imaging system, Dr. William Anderson, Xenogen Corporation, November 17, 2005.
3. Workshop: Theory and practical training on MRI and MRS. Dr. Paul Wang, September, 2005.
4. Seminar: Biophotonic imaging and its uses for monitoring and tracking disease processes in live animals, Dr. Alexandra De Lille, Xenogen Corporation. November 10, 2005.
5. Seminar: Application of Imaging Modalities in Basic Research and Clinical Investigations, Dr, Dnyanesh N. Tipre, NIH/NCI, May 5, 2006.
6. Seminar: Live cell imaging of endocytosis and the intercellular trafficking of multifunctional lipid nanoparticles. Dr. Tieqiao Zhang, NIH, May 10, 2005

II.3 Statement of Work

Task 1. To conduct the study "MR Image Enhancement by Tumor Cell Targeted Immunoliposome Complex Delivered Contrast Agent"

a. Purchase supplies for cell culture and materials for construction of liposome (Months 1-2) (**completed**)
b. Construct and measure the size of liposome (Months 3-4) (**completed**).
c. Attach ligands (single chain variable fragment of transferring antibody) to liposome (TfR-scFv-Lip) (Months 5-8) (**completed**).
d. Make TfR-scFv-Lip-contrast agent complex. Measure the size of complex and amount of contrast agent encapsulated in the liposome (Month 9-12) (**completed**).
e. In vitro imaging of transfected MDA-MB-231 breast cancer cells in pellet (Month 13-24).
f. Verify the transfection efficiency by MRI and optical imaging (Month 19-24).
g. Animal Study: Grow tumor xenografts on nude mice. In vivo MRI imaging of 120 tumor-bearing mice administered TfR-scFv-Lip-CA, Lip-CA, and CA only, using T1 and T2 weighted MRI imaging techniques (Months 27-45).
h. Quantify the contrast enhancement. Image data analysis (Months 27-45).

Task 2. To conduct the study "Imaging the Effects of Macrophage Function on Tumor Promotion"

- Determine the effects of macrophages on metastasis-related gene expression in breast cancer cells (Months 1 – 24) (**in progress)**.
  a. Measure migratory and invasive properties of breast cell lines that are co-cultured with macrophages: changes in anchorage-dependent cell growth, invasion through matrigel (Months 1 – 12) (**in progress)**.
  b. Isolate RNA for gene expression analysis using gene arrays. Monitor expression of proinvasive integrins, MMPs, and TIMPs, etc. (Months 6 – 18) (**in progress)**.
  c. Transfect MCF-12A (mammary epithelial cells), MDA-MB-231, and MDA-MB-468 cancer cells with luciferase construct. Screen luciferase-expressing cells and isolate stable clones by limiting dilution (Months 8 – 24) (**in progress)**.

- Determine the effects of co-culture with macrophages on the growth of Luc^+ mammary epithelial cells and breast cancer cells in 20 athymic nu/nu mice (Months 24 – 48).
  a. Luc^+ MCF-7 cells (in development) and MDA-MB-231 cells will be obtained from Xenogen. Luc^+ mammary epithelial and breast cancer cells co-cultured with macrophages (LPS activated or unactivated). Inject breast cells into athymic mice and monitor with the Xenogen IVIS™ Imaging System. (Month 24-48).
  b. Repeat gene expression experiments in Luc^+ cells to correlate gene expression patterns with *in vivo* growth (Months 36 – 48).

Task 3. To establish a molecular imaging core facility.
  a. Purchase laboratory supplies (months 1-4) (**completed**).
  b. Purchase Xenogen IVIS imaging system (months 3-9) (**completed**).
  c. Establish the designated Molecular Imaging Core Facility in Cancer Center (Rm B-103). Install incubator and hood. (Months 3-9) (**completed**).
  d. Relocate/centralize all the molecular biology instruments to the Molecular Imaging Core Facility (Months 3-9) (**completed**).
  e. Training on Xenogen IVIS imaging system (Month 10) (**completed**).
  f. Molecular Imaging Core Facility open house (Month 10) (**completed**).

Task 4. To train faculty trainees in molecular imaging research.
  a. Biweekly group meetings (organized by research leaders) (Months 1-48) (**in progress)**.
  b. Monthly journal clubs (Months 1-48) (**in progress)**.
  c. Seminar series (nine seminars each year) (Months 1-48) (**in progress)**.
  d. Six workshops (chaired by Dr. Wang and Dr. Bhujwalla) (months 1-18) (**in progress)**.
  e. Laboratory Internships (2 days to one week each) (Months 1-18) (**in progress)**.
  f. Research concepts development (Months 24-36).
  g. Research grants submission (Months 37-48).

Task 5. Administrative and communication affairs (coordinated by Dr. Wang and Dr. Bhujwalla). (Months 1-48) (**in progress)**.
  a. Status reports (monthly, quarterly, and annual reports).
  b. Research progress review (quarterly).
  c. Administrative meetings (biannually meetings).
  d. Coordination of seminars, workshops, and laboratory internships.

III. KEY RESEARCH ACCOMPLISHEMENTS

Project 1: MR Image Enhancement by Tumor Cell Targeted Immunoliposome Complex Delivered Contrast Agent

- A dual probe with fluorescent and magnetic reporter groups was constructed by linkage of the near-infrared (NIR) fluorescent transferrin conjugate on the surface of contrast agent-encapsulated cationic liposome (Tf^{NIR}-Lip^{NBD}-CA).
- Confocal microscopy, optical imaging and MRI showed a dramatic increase of *in vitro*

cellular uptake of the fluorescent and magnetic reporter groups from the Tf^{NIR}-Lip^{NBD}-CA probe compared to the uptake of CA or Lip-CA alone.

- Intravenous administration of the dual probe to nude mice significantly enhanced the tumor contrast in MRI and preferential accumulation of the fluorescent signal was clearly seen in NIR-based optical images.
- The contrast enhancement in MRI by the Tf^{NIR}-Lip^{NBD}-CA probe showed a heterogeneous pattern within tumors, which reflected the tumor morphological heterogeneity.

Project 2: Imaging the Effects of Macrophages on Breast Cancer Metastasis

- MCF-7-Luc-F5 cells grown in RPMI Medium 1640 supplemented with 10% FBS and 10 μg/ml bovine insulin, sodium pyruvate and non-essential amino acids, showed significant differences in the growth patterns, compared with the parent MCF-7 cells grown in MEM without insulin, non-essential amino acids, sodium pyruvate and phenol red.
- MCF-7-Luc-F5 cells have a doubling time of 22 hours as compared to 40 hours for the parental MCF-7 cell line.

IV. REPORTABLE OUTCOMES

Research

Reprints (Listed in the Appendices section)

1. Pirollo K, Dagata J, Wang PC, Freedman M, Vladar A, Fricke S, Ileva L, Zhou Q, Chang EH. A Tumor-Targeted Nanodelivery System to Improve Early MRI Detection of Cancer. J Mol Imaging 5(1):41-52, 2006.

Presentations

1. Wang PC, Pirollo K, Song HF, Shan L, Bhujwalla Z, Chang E. Evaluation of Transferrin Receptor Targeted Immunoliposome Contrast Agent Delivery System for In Vivo MR Imaging in Solid Tumor Xenografts. The Society of Molecular Imaging 4th Annual Meeting, September 7-10, 2005, Cologne, Germany.
2. Freedman M, Pirollo K, Fricke S, Wang PC, Chang E. Imaging of pancreatic carcinoma xenografts in athymic nude mice with carcinoma selective transferrin receptor targeting gadopentetate dimeglumine contrast agent. Radiological Society of North America 2005 Annual Meeting, Chicago, IL, Nov 27- Dec 2, 2005.
3. Wang PC. Biomedical applications of MRI and MRS using small animal models. Department of Physiology and Biophysics, Howard University, February 13, 2005.
4. Zhao A, Wang PC, Wang S, Li C, Laurence GG, Teos L, Haddad GE. Effects of ACE-Inhibition on ANG II and IGF-1 signaling during development and regression of eccentric cardiac hypertrophy. FASEB J. 495.3,.A834, 2006

Submitted Pending Grants

1. Investigation of salvianolic acid B nanoparticles in oral cancer. Howard University Mordecai Wyatt Johnson Award, Xinbin Gu (PI), Eric Walter, Paul Wang.
2. Salvia miltiorrhiza Bge as a new chemopreventive agent for oral cancer, NIH (PR-05-152), Xinbin Gu (PI), Hongguang Ji, Xiaowu Pang, Rajagopalan Sridhar, Paul Wang

3. Development of a MRI and optical dual nanoprobe targeting estrogen receptor (ER) for ER evaluation and breast cancer detection in vivo, USAMRMC 2005 BCRP, Liang Shan, Paul Wang
4. Tumor-targeted MR contrast enhancement using molecular imaging Technique. NIH, Paul C Wang, Zaver M Bhujwalla
5. Salvianolic acid B nanoparticles in prostate cancer chemoprevention and treatment, USAMRMC 2006 PCRP, Xinbin Gu (PI), Eric Walters, Kimberly Jones, Paul Wang

Established Infrastructure

We have established a Molecular Imaging Lab, which includes a newly acquired optical imaging instrument (Xenogen IVIS 200) through this funding and two MRI machines. Pictures of the lab including these imaging machines are posted in the Appendices. The staff of the Molecular Imaging Lab includes an imaging scientist, a molecular biologist, and a research assistant.

V. CONCLUSIONS

In the first year of this training grant, five faculty members from different departments at the Howard University were trained in molecular imaging with the faculty at the In Vivo Cellular Molecular Imaging Center at the Johns Hopkins University. Two research projects have started and progressed well. We have constructed a near-infrared fluorescent transferrin conjugated, contrast agent-encapsulated cationic liposome. This probe has been used to demonstrate a dramatic uptake increase of fluorescent dye and MRI contrast agent both in vitro and in vivo. In the second research project, we have shown a significant different growth pattern between the MCF-7-Luc-F5 cells and its parental MCF-7 cells. The genetic differences and its impact on tumor aggressiveness are under investigated. We have established a Molecular Imaging Laboratory, which is served as a university core facility. Major optical imaging equipment, Xenogen IVIS 200, was acquired through this funding. The Molecular Imaging Lab is staffed with an imaging scientist, a molecular biologist, a pharmacologic chemist, and a research assistant. The lab has a regular bi-weekly group meetings, journal club, and seminars. In addition, three special workshops and three guest seminars on MRI and optical imaging were organized. The trainees have attended various seminars and a one-day retreat at JHU. The PI and the partnership leader have been coordinating the training efforts through meetings and emails. One paper has published and another manuscript is under reviewed.

VI. Abbreviations

CA	contrast agent
FBS	fetal bovine serum
Gd	gadolinium
hTfR	human transferrin receptor
HU	Howard University
ICMIC	In Vivo Cellular Molecular Imaging Center
JHU	John Hopkins University
Lip	liposome
Luc+	luciferase-positive
MEM	minimum essential medium
MR	magnetic resonance
MRI	magnetic resonance imaging
MSR	macrophage scavenger receptor
NIR	near infrared dye
NMR	nuclear magnetic resonance
PBS	phosphate bovine solution
PET	positron emission tomography
RPMI	medium developed at Rosewell Park Memorial Institute
scFv	single-chain antibody variable fragment
Tf	transferrin
Tf^{NIR}	transferrin labeled with near infrared dye
TfR	transferrin receptor
TfR-scFv-Lip	transferrin-single chain variable fragment-liposome
TfR-scFv-Lip-CA	transferrin-single chain variable fragment-liposome-contrast agent

VII. REFERENCES

1. Weissleder R, Mahmood U. Molecular Imaging. Radiology 219:316-333, 2001.
2. Sharma V, Luker GD, Piwnica-Worms D. Molecular imaging of gene expression and protein function *in vivo* with PET and SPECT. J Magn Reson Imag 16:336-351, 2002
3. Louise AY, Huber MM, Ahrens ET, Rothbacher U, Moats R, Jacobs RE, Fraser SE, Meade TJ. In vivo visualization of gene expression using magnetic resonance imaging. Nature Biotechnology 18:321-325, 2000.
4. Kayyem JF Kumar RM, Fraser SE, Meade TJ. Receptor-targeted co-transport of DNA and magnetic resonance contrast agents. Chemistry and Biology 2:615-620, 1995.
5. Pautler RG (2004). Mouse MRI: concepts and applications in physiology. *Physiol*. 19:168-175.
6. Artemov D (2003). Molecular magnetic resonance imaging with targeted contrast agent. *J Cell Biochem*. 90: 518-524.
7. Massoud TF, Gambhir SS (2003). Molecular imaging in living subjects: seeing fundamental biological processes in a new light. *Gene Dev*. 17:545-580.
8. Persigehl T, Heindel W, Bremer C (2005). MR and optical approaches to molecular imaging. *Abdom Imaging*. 30:342-354.
9. Blasberg RG (2003). Molecular imaging and cancer. *Mol Cancer Ther*. 2:335-345.
10. Funovics MA, Kapeller B, Hoeller C, Su HS, Kunstfeld R, Puig S, Macfelda K (2004). MR imaging of the her2/neu and 9.2.27 tumor antigens using immunospecific contrast agents. *Magn Reson Imaging*. 22:843-850.
11. Basilion JP (2001). Current and future technologies for breast cancer imaging. *Breast Cancer Res*. 3:14-16.
12. Artemov D, Mori N, Okollie B, Bhujwalla ZM (2003). MR molecular imaging of HER-2/neu receptor in breast cancer cells using targeted iron oxide nanoparticles, *Magn Reson Med*. 49:403-408.
13. Mulder WJM, Strijkers GJ, Griffioen AW, van Bloois L, Molema G, Storm G, Koning GA, Nicolay K (2004). A liposomal system for contrast-enhanced magnetic resonance imaging of molecular targets. *Bioconjugate Chem*. 15:799-806.
14. Graves EE, Weissleder R, Ntziachristos V (2004). Fluorescence molecular imaging of small animal tumor models. *Curr Mol Med*. 4:419-430.
15. Ntziachristos V, Bremer C, Weissleder R (2003). Fluorescence imaging with near-infrared light: new technological advances that enable in vivo molecular imaging. *Eur Radiol*. 13:195-208.
16. Hoffman RM (2005). The multiple uses of fluorescent proteins to visualize cancer in vivo. *Nature* 5:796-806.
17. Schellenberger EA, Sosnovik D, Weissleder R, Josephson L (2004). Magneto/optical annexin V, a multimodal protein. *Bioconjugate Chem*. 15:1062-1067.
18. Blasberg RG (2003). In vivo molecular-genetic imaging: multi-modality nuclear and optical combinations. *Nucl Med Biol*. 30:879-888.
19. Veiseh O, Sun C, Gunn J, kohler N, Gabikian P, Lee D, Bhattarai N, Ellenbogen R, Sze R, Hallahan A, Olson J. Zhang M (2005). Optical and MRI multifunctional nanoprobe for targeting gliomas. *Nano Lett*. 5:1003-1008.

20. Jones DT, Trowbridge IS, Harris AL (2006). Effects of transferrin receptor blockade on cancer cell proliferation and hypoxia-inducible factor function and their differential regulation by ascorbate. *Cancer Res*. 66:2749-2756.
21. Hogemann-Savellano D, Bos E, Blondet C, Sato F, Abe T, Josephson L, Weissleder R, Gaudet J, Sgroi D, Peters PJ, Basilion JP (2003). The transferrin receptor: a potential molecular imaging marker for human cancer. *Neoplasia*. 5:495-506.
22. Xu L, Pirollo KF, Tang Wh, Rait A, Chang EH (1999). Transferrin-liposome-mediated systemic p53 gene therapy in combination with radiation results in regression of human head and neck cancer xenographs. *Hum Gene Ther*. 10:2941-2952.
23. Bellocq NC, Pun SH, Jensen GS, Davis ME (2003). Transferrin-containing, cyclodextrin polymer-based particles for tumor-targeted gene delivery. *Bioconjugate Chem*. 14:1122-1132.

VIII. APPENDICES

1. Pirollo K, Dagata J, Wang PC, Freedman M, Vladar A, Fricke S, Ileva L, Zhou Q, Chang EH. A Tumor-Targeted Nanodelivery System to Improve Early MRI Detection of Cancer. J Mol Imaging 5(1):41-52, 2006.
2. Shan L, Wang S, Sridhar R, Bhujwalla ZM, Wang PC. Dual Probe with Fluorescent and Magnetic Properties for Imaging Solid Tumor Xenografts. J Mol Imaging (submitted)
3. Pictures of the MRI machines and the Xenogen optical imaging instrument.

A Tumor-Targeted Nanodelivery System to Improve Early MRI Detection of Cancer

Kathleen F. Pirollo[1], John Dagata[2], Paul Wang[3], Matthew Freedman[1], Andras Vladar[2], Stanley Fricke[1], Lilia Ileva[1], Qi Zhou[1], and Esther H. Chang[1]

[1]Georgetown University Medical Center, [2]National Institute of Standards and Technology, and [3]Howard University

Abstract

The development of improvements in magnetic resonance imaging (MRI) that would enhance sensitivity, leading to earlier detection of cancer and visualization of metastatic disease, is an area of intense exploration. We have devised a tumor-targeting, liposomal nanodelivery platform for use in gene medicine. This systemically administered nanocomplex has been shown to specifically and efficiently deliver both genes and oligonucleotides to primary and metastatic tumor cells, resulting in significant tumor growth inhibition and even tumor regression. Here we examine the effect on MRI of incorporating conventional MRI contrast agent Magnevist® into our anti-transferrin receptor single-chain antibody (TfRscFv) liposomal complex. Both in vitro and in an in vivo orthotopic mouse model of pancreatic cancer, we show increased resolution and image intensity with the complexed Magnevist®. Using advanced microscopy techniques (scanning electron microscopy and scanning probe microscopy), we also established that the Magnevist® is in fact encapsulated by the liposome in the complex and that the complex still retains its nanodimensional size. These results demonstrate that this TfRscFv–liposome–Magnevist® nanocomplex has the potential to become a useful tool in early cancer detection. *Mol Imaging* (2006) **5,** 41–52.

Keywords: Nanocomplex, tumor targeting, Magnevist®, MRI, early detection.

Introduction

The ability to detect cancer, both primary and metastatic disease, at an early stage would be a major step toward the goal of ending the pain and suffering from the disease. The development of tumor-targeted delivery systems for gene therapy has opened the potential for delivery of imaging agents more effectively than is currently achievable. Magnetic resonance imaging (MRI) can acquire 3-D anatomical images of organs. Coupling these with paramagnetic images results in the accurate localization of tumors as well as longitudinal and quantitative monitoring of tumor growth and angiogenesis [1,2].

One of the most common paramagnetic imaging agents used in cancer diagnostics is Magnevist® (gadopentetate dimeglumine). Gadolinium is a rare earth element. It shows paramagnetic properties because its ion (Gd^{2+}) has seven unpaired electrons. The contrast enhancement observed in MRI scans is due to the strong effect of Gd^{2+} primarily on the hydrogen-proton spin–lattice relaxation time (T1). Whereas free gadolinium is highly toxic and thus unsuitable for clinical use, chelation with diethylenetriamine pentacetic acid generates a well-tolerated, stable, strongly paramagnetic complex. This metal chelate is metabolically inert. However, after intravenous (iv) injection of gadopentetate dimeglumine, the meglumine ion dissociates from the hydrophobic gadopentetate, which is distributed only in the extracellular water. It cannot cross an intact blood–brain barrier and therefore does not accumulate in normal brain tissue, cysts, postoperative scars, etc, and it is rapidly excreted in the urine. It has a mean half-life of about 1.6 hr. Approximately 80% of the dose is excreted in the urine within 6 hr.

A systemically administered tumor-targeting delivery system has been developed in our laboratory for use in gene medicine [3–8]. This nanosized complex is composed of a cationic liposome encapsulating the nucleic acid payload, which can be either genes [3–6] or oligonucleotides [7,8]. Decorating the surface of the liposome is a targeting molecule that can be a ligand, such as folate or transferrin, or an antibody or an antibody fragment directed against a cell surface receptor. The presence of the ligand/antibody on the liposome facilitates the entry of the complex into the cells through binding of the targeting molecule by its receptor followed by internalization of the bound complex via receptor-mediated endocytosis, a highly efficient

Abbreviations: Lip, liposome; Mag, Magnevist® (Gadopentetate Dimeglumine); SEM, scanning electron microscopy; SPM, scanning probe microscopy; STEM, scanning transmission electron microscopy; TfRscFv, anti-transferrin receptor single chain antibody; TfRscFv-Lip-Mag, anti-transferrin receptor single chain antibody-liposome-Magnevist® complex.

Corresponding author: Esther H. Chang, PhD, Department of Oncology, Lombardi Comprehensive Cancer Center, Georgetown University Medical Center, 3970 Reservoir Road, NW, The Research Building, TRB E420, Washington, DC 20057-1460; e-mail: change@georgetown.edu.

Received 25 February 2005; Received in revised form 8 June 2005; Accepted 17 June 2005.
DOI 10.2310/7290.2006.00005

internalization pathway [9,10]. This modification of the liposomes results in their being able to not only selectively deliver their payload to tumor cells, but also increases the transfection efficacy of the liposome. Transferrin receptor (TfR) levels are elevated in various types of cancer including oral, prostate, breast, and pancreas [11–16]. Moreover, the TfR recycles during internalization in rapidly developing cells such as cancer cells [16], thus contributing to the uptake of these transferrin-targeted nanocomplexes even in cancer cells where TfR levels are not elevated. The nanocomplex used in the studies described here uses an anti-transferrin receptor single-chain antibody fragment (TfRscFv) as the targeting moiety [17,18]. TfRscFv contains the complete antibody-binding site for the epitope of the TfR recognized by the monoclonal antibody 5E9 [18]. TfRscFv has advantages over the transferrin molecule itself, or an entire monoclonal antibody, in targeting liposomes to cancer cells with elevated TfR levels: (1) The size of the scFv (28 kDa) is much smaller than that of the transferrin molecule (80 kDa) or the parental monoclonal antibody (155 kDa). The scFv liposome–DNA complex may thus exhibit better penetration into small capillaries characteristic of solid tumors. (2) The smaller scFv has a practical advantage related to the scaled-up production necessary for the clinical trials. (3) The scFv is a recombinant molecule and not a blood product like transferrin and thus presents no danger of a potential contamination by blood-borne pathogens. (4) Without the Fc region of the monoclonal antibody, the issue of non-antigen-specific binding through Fc receptors is eliminated [19]. Most importantly, we have already shown that such an anti-TfR single-chain antibody molecule can target an intravenously administered cationic liposome–DNA nanocomplex preferentially to tumors [5,6]. Encapsulating Magnevist® within such a tumor-targeted nanocomplex offers potential advantages for enhanced sensitivity, detection of metastases, and diagnosis of cancer.

In this article, using a mouse xenograft model of human pancreatic cancer, we explore the use of this nanocomplex for systemic delivery of the imaging agent Magnevist® to tumors. In addition, we used scanning electron microscopy (SEM) and scanning probe microscopy (SPM) [20–25] to examine the physical structure and size of these Magnevist®-carrying nanocomplexes. Because gadolinium is a high-atomic-number element and possesses a large magnetic moment, these properties can be exploited in a variety of ways to enhance contrast in both SEM and SPM. The findings presented below demonstrate that our ligand–liposome nanocomplex does indeed encapsulate Magnevist® and that iv administration of this complex results in enhanced tumor imaging.

Materials and Methods

Cell Lines

Human lymphoblastic leukemia cell line K562 was obtained from the Lombardi Comprehensive Cancer Center Tissue Culture core facility (Washington, DC). These suspension cells were maintained in RPMI 1640 supplemented with 10% heat-inactivated fetal bovine serum (FBS) plus 2 mM L-glutamine, and 50 μg/mL each of penicillin, streptomycin, and neomycin. Human pancreatic cancer cell line CaPan-1 (obtained from ATCC, Manassas, VA) was derived from a metastatic adenocarcinoma of the pancreas. It was maintained in Iscove's modified Dulbecco's medium containing 4 mM L-glutamine and sodium bicarbonate, supplemented with 20% non-heat-inactivated FBS, 2 mM L-glutamine, and 50 μg/mL each of penicillin, streptomycin, and neomycin. Human prostate cancer cell line DU145 (ATCC) was originally derived from a lesion in the brain of a patient with widespread metastatic carcinoma of the prostate. It was maintained in minimum essential medium with Earle's salts supplemented with 10% heat-inactivated FBS plus L-glutamine and antibiotics as above.

Nanocomplex Formation

Cationic liposome (DOTAP:DOPE) was prepared by the ethanol injection method as previously described [6]. When delivering plasmid DNA, the full complex was formed in a manner identical to that previously described [26]. To encapsulate the imaging agent, the TfRscFv was mixed with the liposome at a specific ratio (identical to that used with DNA) and incubated at room temperature for 10 min. Magnevist® was added to this solution, mixed, and again incubated at room temperature for 10 min. When stored at 2–8°C the complex is stable for at least 8 days, as determined by size measurements using a Malvern Zetasizer 3000H (Malvern, UK). The average of the cumulants (Z average) measurements over this time frame is 112.3 ± 4.67 (*SE*), whereas the polydispersity (representing the reproducibility of the values during repeat scans) is 0.445 ± 0.03. For in vitro transfection, 2 mL of serum-free medium was added to the complex before transfection. When prepared for in vivo use, dextrose was added to a final concentration of 5%. For both in vitro and in vivo complex formation, the ratio of Magnevist® to liposome was 1:7 (vol/vol).

In Vitro Transfection

To transfect suspension cells K562, 15×10^6 cells in a total volume of 4.0 mL of medium with all supplements except serum (serum-free medium) were placed into a 100-mm^2 tissue-culture dish. Two milliliters of the transfection solution from above, containing varying amounts of Magnevist®, was added to the cell suspension. The plate was incubated at 37°C with gentle rocking for the length of time given in the Results section (up to 90 min), after which the cells were gently pelleted ($600 \times g$ for 7 min) at 4°C in 0.5 mL microcentrifuge tubes and washed three times with 10 mL of serum free medium to remove any excess transfection solution and placed on wet ice until imaged.

In Vivo Tumor Targeting

To assess the tumor-selective targeting of the TfRscFv–liposome (TfRscFv–Lip) nanocomplex to primary and metastatic tumors, an orthotopic metastasis model using human pancreatic cancer cell line CaPan-1 was used. Subcutaneous xenograft tumors of CaPan-1 were induced in female athymic nude mice by injection of 1×10^7 CaPan-1 cells suspended in Matrigel collagen basement membrane matrix (BD Biosciences, San Jose, CA). Approximately 8 weeks later, the tumors were harvested and a single-cell suspension of the tumor was prepared. Cells ($1.2–1.5 \times 10^7$), also suspended in Matrigel were injected into the surgically exposed pancreas of female athymic nude mice as previously described [27]. Five weeks post surgery, the complex carrying the *LacZ* gene was iv injected 3× over 24 hrs (at 40 μg DNA per injection). Sixty hours later, the animals were sacrificed and examined for the presence of metastases and organs stained for β-galactosidase expression using a previously described procedure [3].

Magnetic Resonance Imaging

For in vitro MRI, the cell pellets in microcentrifuge tubes were positioned at the center of the magnet. The MRI was performed at Howard University using a 4.7-T horizontal bore NMR machine (Varian Inc, Palo Alto, CA). The imaging protocols consist of a multislice T1-weighted spin–echo imaging sequence and a saturation–recovery sequence. For the T1-weighted imaging technique, the repetition time (TR) was 1000 msec and the echo time (TE) was 13 msec. The T1-weighted spin–echo imaging technique was applied to verify the positive image enhancement. The saturation–recovery MR sequence with variable echo times was used for the T1 measurement. The slice thickness of images was 0.5 mm. The radiofrequency (RF) coil used was a 30-mm single-loop coil. The RF coil serves as an RF transmitter and receiver. The RF pulse was a selective 5-msec sinc pulse. The number of phase-encoding steps was 256. The field of view was 15 × 15 mm. The image area chosen in the study was at the center of the RF coil for RF homogeneity. The MR images were taken in the cross-section direction of the microcentrifuge tube. The height of the cell pellet was 12 mm. The range of the multislice images covers the whole pellet. The center slice images, which were not influenced by the image distortion due to the susceptibility effect from the air–pellet boundary, were used for the studies. The image intensity was measured using the Varian Image Browser software. The signal is taken from a region of interest that is big enough to cover two thirds of the image from each microcentrifuge tube. The relative image intensities of the pellets from these tubes were applied for contrast enhancement evaluation and the T1 measurements.

For the in vivo studies, mice bearing CaPan-1 orthotopic tumors or DU145 subcutaneous xenograft tumors were used. The CaPan-1 tumors were induced as described above. DU145 tumors were induced by the subcutaneous inoculation of 7×10^6 cells in Matrigel. These studies were performed at Georgetown University. Animals to be imaged were anesthetized and placed in a proprietary, in-house designed, animal management system. This system incorporates a warm-water heating system that maintains the temperature at 37°C, as well as a four-channel, thermal optical monitoring system used to monitor animals' skin temperature, ambient temperature, and wall temperature of the device. For imaging, anesthesia was induced using isoflurane at 4%, with the remaining gas composed of a 66% oxygen and 30% nitrous oxide mixture. Maintenance of anesthesia was achieved with 1.5% isoflurane under similar gaseous conditions of oxygen and nitrous oxide as noted. The anesthetized animal was positioned inside a cylindrical, variable RF resonant antenna (birdcage resonator volume coil) and tuned to a center frequency of approximately 300 MHz (the resonant frequency of water molecules when subject to a field strength of 7 T). The imaging protocol used was T1-weighted Turbo-RARE (rapid acquisition with rapid enhancement) 3-D imaging sequences performed on a 7T Bruker BioSpin (Billerica, MA) imaging console. The imaging parameters used were as follows: T1-weighted Turbo-RARE 3-D, TE 13.3 msec, TR 229.5 sec, flipback on, four echoes with a field of view of 8.0/3.5/3.5 cm and a 256 × 256 × 256 matrix. After a baseline image was acquired, the animal was kept immobilized in the animal holder and the Magnevist® only [diluted to 400 μL with 1× phosphate-

buffered saline (pH = 7.4)] or the TfRscFv–Lip–Mag complex (total volume 400 μL) was systemically administered using a 27 G needle by iv injection into the tail vein of the animal and the 3-D imaging sequence was immediately initiated. The imaging with the two solutions were performed on sequential days.

Scanning Electron Microscopy

Sample solutions of liposome-encapsulated Magnevist contrast agent and complete nanocomplex consisting of a tumor-targeting single-chain transferrin receptor protein coating the liposome-encapsulated complex, TfRscFv–Lip–Mag, were prepared at Georgetown University Medical Center (GUMC), delivered to National Institute of Standards and Technology (NIST) and were stored under dark and refrigeration. For each imaging session, a fresh dilution 1:3 by volume with deionized water was prepared and a 5-μL droplet was micropipetted onto a standard 200-mesh transmission electron microscopy grid consisting of 30–60 nm formvar and 15–20 nm carbon. The droplet was allowed to dry on the grid in air for 5 min before being loaded into the vacuum chamber of the microscope. Imaging was performed using a Hitachi S-4800 field-emission microscope at NIST. Of particular interest to applications of SEM to nanocomplex imaging is a comparison of upper and lower secondary electron detectors [SE9(U) and SE(L)]—using the SEM in its usual mode—to the addition of a transmitted electron (TE) detector, transforming the instrument into a low-voltage STEM.

Scanning Probe Microscopy

Sample solutions of liposome-encapsulated Magnevist contrast agent and complete nanocomplex were prepared at GUMC, delivered to NIST, and were stored under dark and refrigeration. For each imaging session, a fresh dilution 1:3 by volume with deionized water was prepared and a 5-μL droplet was micropipetted onto an untrasonically cleaned silicon substrate used with native oxide or with a poly-L-lysine coating. SPM imaging were obtained using a Veeco (Santa Barbara, CA) MultiMode microscope with a Nanoscope IV controller. Topography by tapping mode with Z control [Veeco RTESP cantilevers, of approximately 320–360 kHz and *k* approximately 20–60 N/m], phase imaging, and magnetic force microscopy using magnetic-coated tips (Veeco MESP 68 kHz] were performed in life mode. Dynamic imaging of dewetting and surface energy "phase separation" as the solution evaporates to expose isolated nanoparticles and aggregates were used to understand the consequences of solvent drying on the stability of the particles and its effect on the various SPM contrast mechanisms available with the SPM system.

Results

Tumor-Specific Targeting by the Ligand–Liposome Nanocomplex Carrying a Reporter Gene

To assess selective targeting of the TfRscFv–LipA nanocomplex to primary tumor and metastases, an orthotopic metastasis model, a closer approximation of the clinical situation, using human PanCa cell line CaPan-1 was used. Surgical orthotopic implantations of CaPan-1 xenograft tumor sections into nude mice have been shown to produce, within 56 days, metastases in liver and spleen [27]. Orthotopic tumors of CaPan-1 were induced in female athymic nude mice as described in Materials and Methods. Approximately 5 weeks later, the animals were euthanized and necropsied to look for tumor in the pancreas and other organs. As shown in Figure 1A, extensive tumor growth is evident throughout the pancreas. Metastases were present in various organs in four of five mice including the spleen, liver, lung, adrenal gland and even within the diaphragm. This experiment was repeated with similar results.

To establish selective targeting tumor and metastasis, before sacrificing the mice, the TfRscFv–LipA complex carrying pSVb (LacZ) plasmid DNA for β-galactosidase expression was iv injected into the mice three times over a 24-hr period (40 μg of plasmid DNA per injection). All five mice were sacrificed 60 hr after injection and various organs, including the liver, lung, spleen, pancreas and

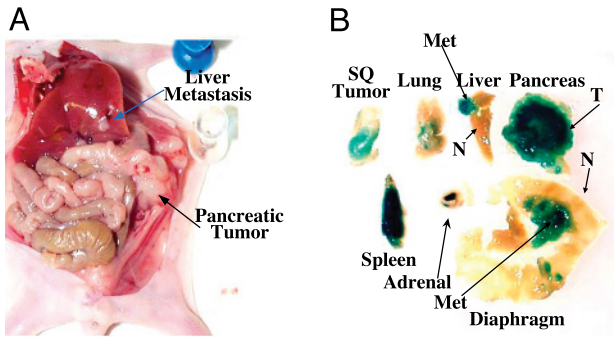

Figure 1. *Tumor-specific targeting of a CaPan-1 orthotopic metastasis model by the TfRscFv–Lip–DNA nanocomplex. Subcutaneous CaPan-1 xenograft tumors were induced in female athymic nude mice as described in Materials and Methods. The tumors were harvested and a single-cell suspension in Matrigel was injected into the surgically exposed pancreas. Five weeks post injection, the TfRscFv–Lip complex carrying the LacZ gene for β-galactosidase expression (40 μg) was iv injected 3× over 24 hr. Sixty hours later, the animals were sacrificed and examined for the presence of metastases and the organs stained for β-galactosidase expression. The same tumor nodule in the liver indicated by an arrow in A exhibits intense β-galactosidase expression in B. (A) Gross necropsy; (B) tissues after staining for β-galactosidase.*

diaphragm, were harvested and examined for the presence of metastasis and tumor-specific staining. Fresh samples, sliced at 1-mm thickness, were stained with X-gal to produce a blue color where the gene is expressed. The tumor-targeting ability and high transfection efficiency of the complex is demonstrated by the presence of the reporter gene in the various organs from this animal (Figure 1B). In the liver, lung, adrenal gland, and diaphragm, it is clearly shown that the reporter gene is highly expressed only in the metastases, whereas in the adjacent normal tissue, no blue color is evident. The metastasis visible in the liver in Figure 1A (arrow) is the same tumor nodule strongly expressing β-galactosidase in Figure 1B (arrow) confirming the tumor-specific nature of this nanocomplex. In some of the mice, growth of the tumor in pancreas also resulted in extrusion of tumor through the original incision site used for implantation. In Figure 1B, this strongly blue stained subcutaneous tumor, surrounded by normal nonstained skin, is also shown, again showing tumor cell specificity. Similar results were observed in the rest of the mice and in the repeat experiment. Thus, this systemically administrated nanocomplex will target tumor cells, both primary and metastatic, wherever they occur in the body, and efficiently deliver plasmid DNA. We wished to expand the potential of this delivery system to include contrast agents. The ability to do so could result in improved imaging and cancer detection.

In Vitro Studies Using TfRscFv–Lip Complex to Deliver Magnevist®

As Magnevist® is one of the most frequently used contrast agents in the clinic, it was chosen for use in these studies. In our initial experiments, we examined whether the complex could be prepared with Magnevist® and if doing so would enhance the MRI signal. Because trypsinization could lead to membrane damage and leakage of contrast agent from the cells, adherent cells were not used in these studies. Instead, a human lymphoblastic leukemia cell line, K562, which grows as a suspension culture was used. Moreover, gentle pelleting and washing of the cells would remove any excess Magnevist® or complex before imaging, allowing only cell-associated signal to be detected.

Time-Dependent Image Enhancement by the TfRscFv–Lip–Mag Nanocomplex

We examined the optimal time for transfection of the TfRscFv–Lip–Mag nanocomplex. The suggested clinical dose of Magnevist is 0.1 mmol/kg. In these initial studies, we used a dose of 0.3 mmol/kg (corrected for the smaller weight and blood volume of mouse vs. man) in the complex per 250 μL of transfection solution. K562 cells were transfected for times ranging from 20 to 90 min. Twenty minutes showed very low transfection activity based on the image intensity (data not shown). However, as shown in Figure 2A, by 60 min the cells transfected with the complex showed a large increase in intensity as compared to the untreated cells. The intensity of the untreated cells (202 ± 48) was not significantly different from that of an empty marker tube (194 ± 43), indicating that the cells themselves do not contribute to the signal detected. More importantly, the transfection efficiency plateaus at approximately 60 min because the relative intensity of the cells transfected for 60 and 90 min were identical (317 ± 46 and 317 ± 47, respectively).

Magnevist® Dose-Dependent Image Enhancement

Using 60 min as the transfection time, we then assessed the effect of increasing amounts of Magnevist® on the TfRscFv–Lip–Mag complex image enhancement. The doses tested were 0.05, 0.3, and 0.9 mmol/kg. Corrected for size and blood volume of the mouse, the volumes of Magnevist® used in the complex per 250 μL of transfection solution were 0.25, 1.5, and 4.5 μL. As shown in Figure 2B and Table 1, the image intensity increases and the T1 relaxation time shortens as a function of the amount of contrast agent included in the complex.

Image Enhancement by TfRscFv–Lip–Mag as Compared to Free Magnevist®

Based on the above experiments it appears that the TfRscFv–Lip can complex with Magnevist® and deliver it to the cells for image enhancement. To assess the level of enhancement of the complexed contrast agent as compared to the agent alone and demonstrate that the signal obtained is not due to the presence of unincorporated Magnevist®, we treated K562 cells with either free Magnevist® or the TfRscFv–Lip–Mag nanocomplex. The identical amount of contrast agent (0.3 mmole/kg or 1.5 μL/250 μL transfection volume) and transfection time (60 min) was used for both solutions. Whereas free Magnevist® showed enhanced contrast relative to the untreated cells as expected, the cells treated with the TfRscv–Lip–Magnevist complex demonstrated a much greater increase in image intensity and shortened T1 relaxation time compared to both untreated and free-Magnevist®-treated cells (Figure 2C, Table 2). These results not only demonstrate the increased efficiency of contrast agent uptake by means of the targeted nanocomplex, but also indicate that the observed signal is

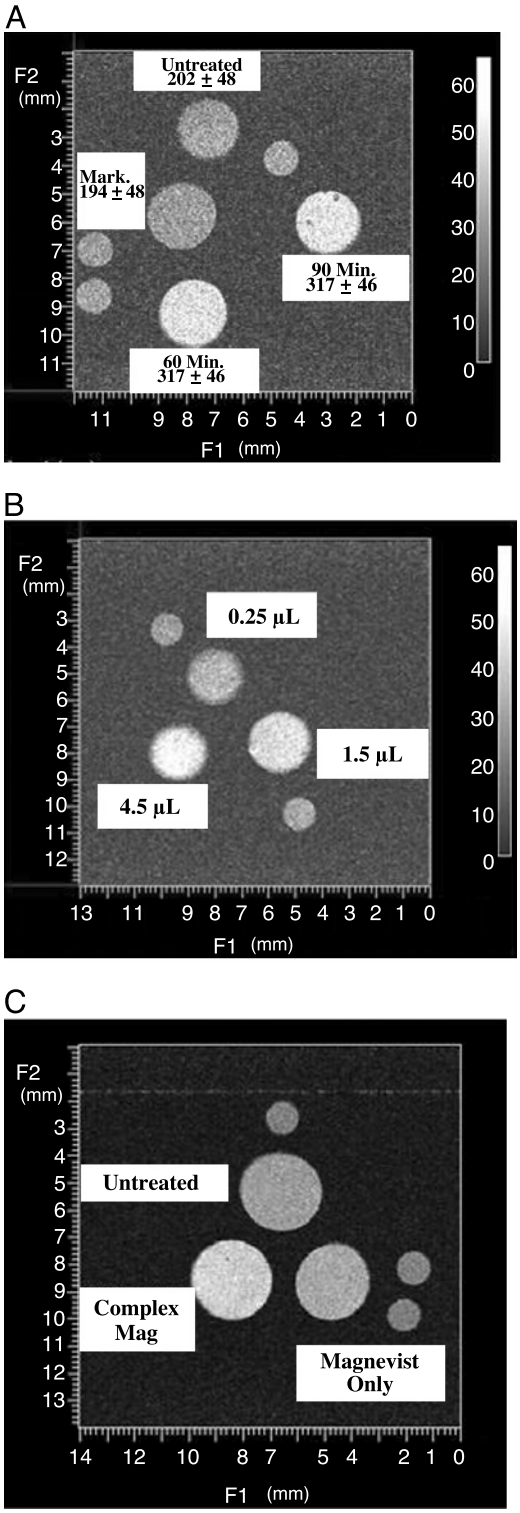

Figure 2. *In vitro MRI of K564 cells after transfection with the TfRscFv–Lip–Mag nanocomplex. After transfection with either free Magnevist® or the noncomplex encapsulating Magnevist® the cells were pelleted and washed with serum-free medium, and MRI performed using a 4.7T Varian NMR. The imaging protocol consisted of T1-weighted spin–echo imaging sequences (TR/TE, 1000/13 msec) to verify the image enhancement and a saturation–recovery MR sequence with variable echo times for the T1 measurement. (A) Time-dependent transfection. The values given are relative intensities. (B) Variation in relative intensity with the amount of Magnevist® included in the complex (in microliters). (C) Comparison of relative intensity of the TfRscFv–Lip–Mag complex versus free Magnevist®. The small circles in all images are markers for sample orientation.*

Table 1. Relative Intensity and T1 Relaxation Time as a Function of Magnevist® in the Complex

Dose of Contrast Agent (mM/kg)	Relative Intensity	T1 (sec)
0.05 (0.25 µL)	293 ± 50	1.43 ± 0.007
0.3 (1.5 µL)	379 ± 43	1.16 ± 0.004
0.9 (4.5 µL)	454 ± 51	1.01 ± 0.004

likely not due to uncomplexed Magnevist®. Further evidence of Magnevist® encapsulation is given below.

In Vivo Image Enhancement with TfRscFv–Lip–Mag

The above studies established that the nanocomplex could more efficiently image tumor cells in vitro than Magnevist® alone. However, to have potential for clinical use, the complex must exhibit a similar effect in vivo. We used the same human pancreatic cancer orthotopic mouse model (CaPan-1) for these studies as was used above to demonstrate tumor-specific targeting of the complex carrying a reporter gene. In addition, a second tumor model, a subcutaneous prostate xenograft mouse model (DU145) was also used. Mice bearing CaPan-1 or DU145 tumors were imaged on a 7T Bruker NMR as described in Materials and Methods. Once positioned in the coil, a baseline image was obtained using a T1-weighted Turbo-RARE 3-D imaging sequence. To facilitate image alignment, after baseline acquisition the animal was maintained in the animal holder while the imaging solution was administered via iv injection. Signal acquisition was begun within 3 min of the injection. The amount of Magnevist® administered to the mouse, either free (as is performed in the clinic) or included in the complex, was 10 µL. This amount is equivalent to 0.2 mmole/kg or twice that used in humans. This amount was selected because the standard human dose of 0.1 mmole/kg Magnevist® alone gave a very poor signal in the mice. The imaging with free Magnevist® and the TfRscFv–Lip–Mag complex were performed on two consecutive days. A baseline scan was also performed before administration of nanocomplex to confirm that all of the Magnevist® from the previous day had been washed out. MR technique and windows were consistent between the two sets of images with the windows

Table 2. Comparison of the Relative Intensity and T1 Relaxation Time between Free and Complexed Magnevist®

Treatment	Relative Intensity	T1 (sec)
Untreated	455 ± 47	1.80 ± 0.009
Free Magnevist®	538 ± 50	1.51 ± 0.007
Complexed Magnevist®	662 ± 52	1.40 ± 0.004

adjusted to correct for an automatic windowing feature of the scanner.

Images of the Magnevist® and nanocomplex–Magnevist in three separate mice are show in Figure 3. In Figure 3A, 4 months after surgical implantation of the CaPan-1 tumor cells, the animal is carrying a large orthotopic tumor. The increased resolution and signal intensity, as compared to the contrast agent alone is quite evident. Similar results are observed in the second mouse with a CaPan-1 tumor shown in Figure 3B. This animal, only 2 months postsurgery, has a visible subcutaneous tumor growing through the site of the incision. A small abdominal mass was also detected by palpation. Not only is the signal in the subcutaneous tumor more enhanced after administration of the complexed Magnevist®, but what appears to be the small orthotopic tumor (arrow) is evident in this scan and not in the one in which the animal received the free Magnevist®. Similarly, increased definition and contrast are evident in the subcutaneous DU145 tumor (Figure 3C) after injection with the TfRscFv–Lip–Mag complex as compared to the free Magnevist®. Reconstruction and quantitation was performed on the images in Figure 3B and C, representing the two different tumor models, pancreatic cancer (CaPan-1) and prostate cancer (DU145). In both instances, there is an increased intensity (pixels) by the free Magnevist® over the baseline, as expected (Table 3). However, delivery of the imaging agent by the tumor-targeting nanocomplex results in an almost threefold further increase in signal intensity in both of these tumor models. These studies thus demonstrate that when Magnevist® is incorporated within the TfRscFv–Lip complex there is an improved tumor visualization in an in vivo situation, and they suggest the potential benefit of further developing this means of tumor detection for clinical use.

Physical Characterization Studies

Whereas the in vitro studies offered circumstantial evidence that complexed Magnevist® is encapsulated

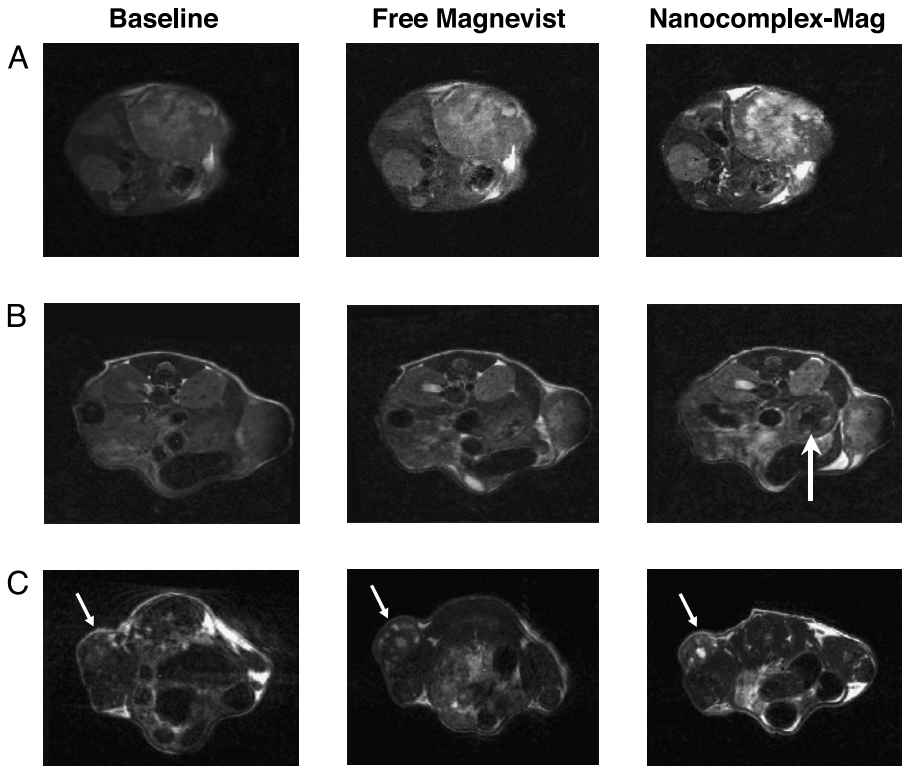

Figure 3. *Improved MRI in two different models of cancer using the ligand–liposome–Mag nanocomplex. Human pancreatic cancer cells (CaPan-1) were surgically implanted into the body of the pancreas, and human prostate cancer cells (DU145) were subcutaneously injected on the lower back of female athymic nude mice. Free Magnevist® or the TfRscFv–Lip nanocomplex containing the same dose of Magnevist® was iv injected (via the tail vein) into each of the three mice on two consecutive days. This amount of Magnevist® is equivalent to twice the dose that would be administered to a human patient. The total volume of solution administered in all cases was 400 μL. A baseline scan was performed just before administration of the nanocomplex to confirm that all of the Magnevist® from the previous day had been washed out. MR technique and windows were constant between the three sets of images, with the windows adjusted to correct for an automatic windowing feature of the scanner. (A) Differences in MRI signal in a large pancreatic orthotopic tumor (arrow) (4 months after surgical implantation of the tumor) between the iv-administered free contrast agent and the TfRscFv–Lip–Mag complex. (B) Similar effect in a second mouse with a subcutaneous pancreatic tumor and a much smaller abdominal pancreatic tumor (arrows). (C) Images of a third animal with a subcutaneous prostate tumor (arrow) in which the same effect is evident.*

Table 3. Intensity Increase over Baseline by Free and Complexed Magnevist®

	CaPan-1	DU145
	% Increase over Baseline	
Complexed Magnevist®	99	215
Free Magnevist®	34.5	70

within the liposome, we have used sophisticated microscopy techniques (SEM and SPM) to confirm this fact and further characterize (e.g., complex size) the TfRscFv–Lip–Mag complex.

Imaging of Liposomes without Magnevist. High-resolution imaging implies narrow depth of focus and so requires relatively thin and flat samples. How thin varies with technique, but surface and substrate effects—surface energy and symmetry lowering—often dominate the structural forces typical of biomaterials. This is particularly true for liposomes given their tenuous nature [28]. So an understanding of reliable methods for preparing and characterizing the dimensional and mechanical stability of isolated liposomes is an essential step. The goal of our present characterization efforts is to perform direct sensing of the mechanical stiffness and magnetic properties of nanoparticles to establish that the contrast agent is indeed contained within the nanoparticle and not simply associated externally with the liposomes.

The SPM images surface topography in tapping mode by oscillating the tip and cantilever to which it is attached close to the cantilever resonance frequency. A feedback circuit maintains the oscillation of the cantilever at constant amplitude. This constant amplitude is given by a set point that is somewhat smaller than that of the freely oscillating cantilever. Because the SPM tip interacts with the surface through various small forces, there is a phase shift between the cantilever excitation and its response at a given point on the surface. For an inhomogeneous surface, the tip–surface interactions will vary according to surface charge, steep topographical changes, and mechanical stiffness variations, for example. By changing the set point and observing how certain features respond to softer or harder tapping, we can correlate this with the response expected for a specific structure such as a liposome. (The free oscillation amplitude signal is approximately 1.78 V.) A sequence of SPM phase images of a pair of isolated liposomes without payload is shown in Figure 4. Figure 4A was imaged at a set point of 1.68 V and the corresponding negative phase difference between the substrate and liposome indicates that the tip–sample interaction is attractive for the liposome, given by a phase value of −3.5°. In the case of an attractive interaction and negative phase, the phase image of the liposome appears dark, except for a topographically keyed ring at the liposome edge. Figure 4B demonstrates the effect of reducing the set point to 1.45 V: The liposome now appears bright because the tip–sample interaction becomes repulsive, and here the phase difference between the liposome and substrate is +8°. Finally, Figure 4C shows that the phase difference recorded at a set point of 1.35 V increases further, becoming +35°.

Imaging of Liposome-Encapsulated Magnevist. Figure 5 presents SPM and SEM images of isolated lipo-

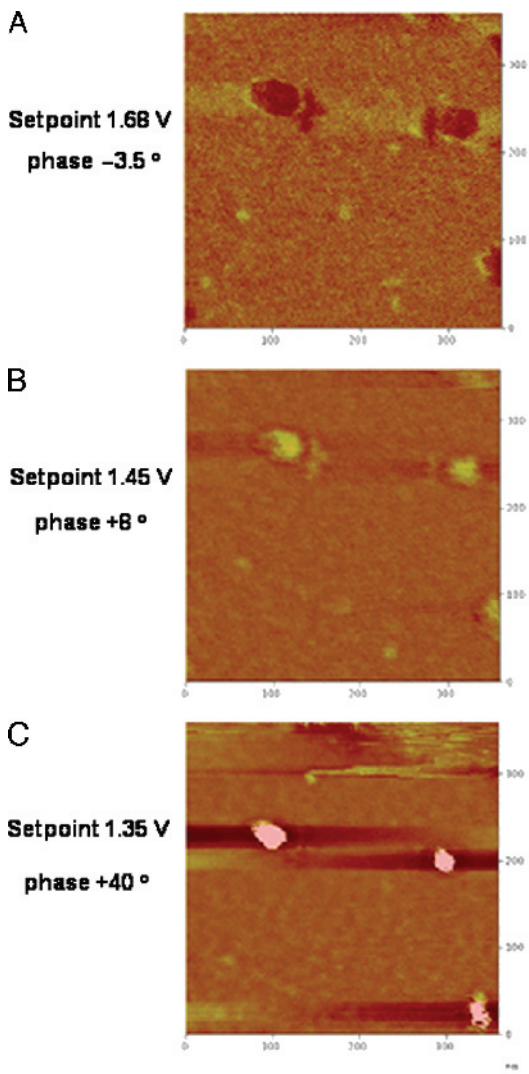

Figure 4. *SPM phase images of liposomes without Magnevist®. The images appearing in A, B, and C were obtained at set points of 1.68, 1.45, and 1.35 V, respectively. The corresponding phase differences between the noncompliant substrate and the mechanically compliant liposome are −3.5°, +8°, and +40°. The interaction of the SPM tip and liposome changes from attractive to repulsive as the set point is decreased.*

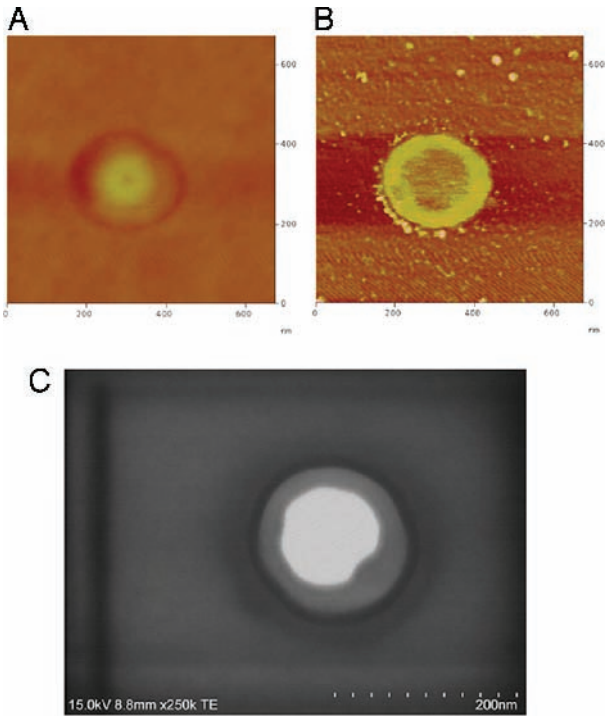

Figure 5. *SPM and SEM images of liposome-encapsulated Magnevist® (Lip+Mag). (A) Atomic force microscopy topographical image of the liposome-encapsulated Magenvist® particle. The SPM phase image (set point = 1.6) (B) and 15 keV SEM (TE) (transmission-mode electron detector) image (C) possess similar contrast, although generated by entirely distinct complementary physical mechanisms.*

some-encapsulated Magnevist (Lip+Mag) nanoparticles. The size distribution of single (Lip+Mag) particles is in the diameter range of 100–200 nm and scales according to optical measurements that indicate that payload-encapsulating liposomes are approximately 50% larger than liposomes alone in their spherical state.

The SPM topograph in Figure 5A indicates that liposomes containing Magnevist have a bimodal surface shape after drying that is more complex than that of the simple elliptical surface of a liposome containing no payload (not shown). The SPM phase behavior differs markedly from that of payloadless liposomes, the outer ring is repulsive relative to the center, and a corresponding SPM phase image is shown in Figure 5B. Regions of both attractive and repulsive tip–sample interaction appear at moderate set point values. A correlation between the SPM phase image obtained at a set point of 1.6 and the SEM image in TE mode is evident in Figure 5B and C. Liposomes appear uniformly bright across the entire particle in SEM images (not shown), similar to the uniform phase images we obtain by SPM. Tips and cantilevers change with time and usage. Moreover, it is important to verify that the images produced are not affected by tip instabilities due to foreign material on the tip. Thus, they are changed frequently. Because each cantilever is somewhat different with respect to its resonance properties, the set points used in Figures 4 and 5 are different.

Imaging of TfRscFv–Lip–Mag Nanocomplex. The complete TfRscFv–Lip–Mag nanocomplex was prepared and imaged by SEM and SPM as described in Materials and Methods. Results, shown in Figure 6 indicate that the solvent film undergoes phase separation; however, examples of isolated NDS can be readily observed on the dried film. Note that the SEM beam clearly causes some damage to the film, but the particles can be repeatedly scanned several times before beam damage becomes significant. The appearance of the full complex is different from that of the (Lip+Mag) only. The shape is less regular and considerable texturing of the liposome surface following drying is consistent with protein denaturation. Also, SEM TE images indicate that the well-defined boundary between the outer ring and center of the liposome seen with the (Lip+Mag) particles is less

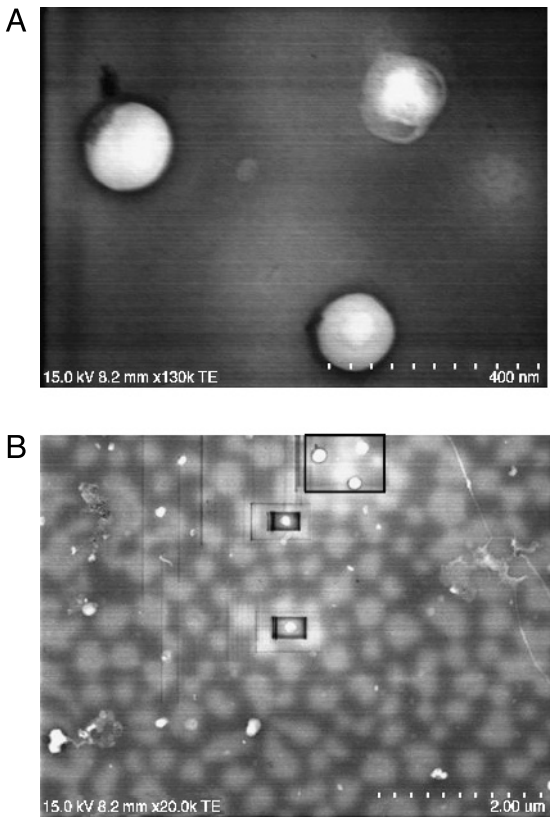

Figure 6. *SPM topographic and phase imaging of TfRscFv–Lip–Mag nanocomplex. (A) 15 keV SEM (TE) (transmission-mode electron detector) image of the full nanocomplex. A suitable choice of amplitude set point readily distinguishes intact nanocomplex particles from decomposition products. It is not known if the decomposed material was present in the solution before sample preparation or is the direct result of interaction with the substrate. (B) power image of the field. The boxed area is the image in A.*

apparent and the shape much more variable. This is consistent with the view that the presence of protein within the liposome has altered the osmotic outflow across the liposome during film drying.

It is possible to obtain additional information about these NDS particles by using the magnetic force microscopy imaging capabilities of the SPM (MFM). Because the magnetic moment of gadolinium-containing Magnevist is quite large, it should be possible using a magnetized SPM tip to interact with the oriented Magnevist concentrated within the liposomes. This is shown in Figure 7 for MFM of several approximately 100- to 200-nm-diameter nanocomplexes. We establish that, in fact, we are producing an image that is truly magnetic in nature by using the lift-mode capabilities of the SPM: In this mode, a topographic image under normal tapping mode conditions is obtained. The reference surface information is then used to offset the tip by a specified height away from the surface and the surface is then scanned at this increased height. This removes the influence of topography on the signal. MFM images obtained in lift mode at a height of 15 nm or more from the surface are given by the magnetic phase image. The appearance of a signal confirms the presence of gadolinium encapsulated within the complex.

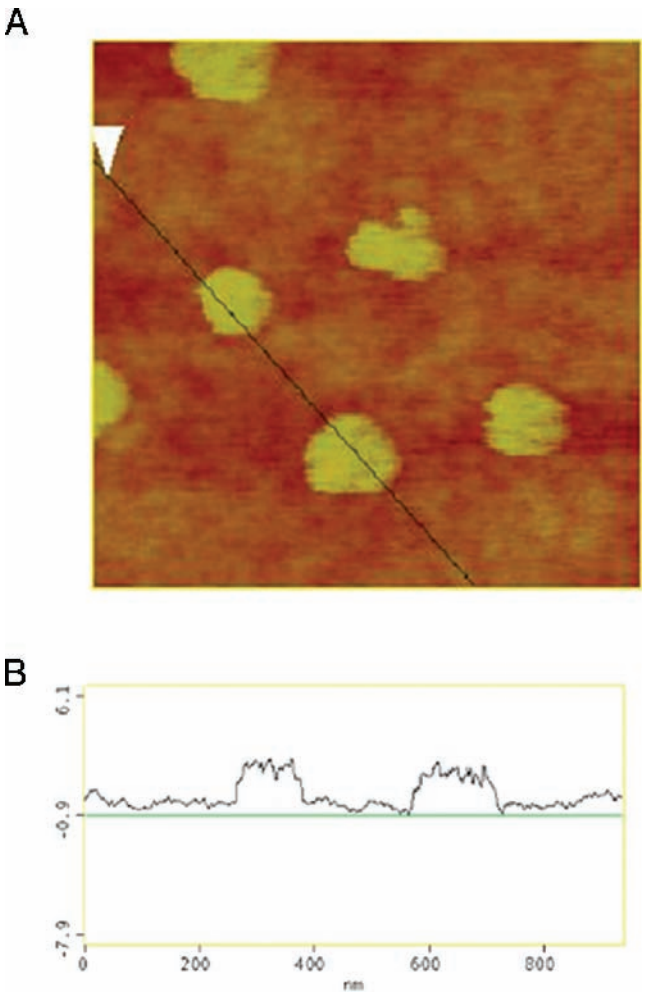

Figure 7. *Cross-sectional comparison of SPM topographic and magnetic phase image in lift mode using 25-nm height displacement. (A) SPM topographic/magnetic phase image of the full TfRscFv–Lip–Mag nanocomplex. The appearance of a double dipole-like signal in B consisting of attractive and repulsive in-plane magnetic interactions suggests that the cause of this interaction is the nonuniform toroidal distribution of Magnevist within the NDS, consistent with SEM and nonmagnetic SPM phase images.*

Discussion

The development of nanoparticle-sized delivery systems that have greater tumor and tissue penetrance is a major direction in medical research in general and cancer research in particular. Combining the capabilities of these small particles with the ability to home specifically to tumor cells wherever they occur in the body could lead to significant advances in cancer treatment and diagnosis. We have previously shown that our ligand–liposome–DNA complex can specifically target and efficiently transfect tumor cells (primary and metastatic) [3–8]. When encapsulating plasmid DNA, this targeted delivery system is truly a nanocomplex, with a uniform size of less than 100 nm [29]. Used in combination with conventional radiation/chemotherapy, delivery of therapeutic genes such as wild-type p53 by means of this nanodelivery system has resulted in tumor growth inhibition and even tumor regression in animal models [3–5,29]. This tumor regression and concomitant decrease in blood flow due to p53-mediated antiangiogenesis have also been demonstrated using Power Doppler ultrasound imaging [30]. Adapting such a tumor-targeted nanocomplex to deliver imaging agents would have the potential to improve early diagnosis as well as detection of metastatic disease. The results described above demonstrate that we can encapsulate and deliver the commonly used MRI agent Magnevist® to tumor cells both in vitro and in an orthotopic animal model and in doing so produce a more defined and intense image than seen with uncomplexed Magnevist®.

Other nanometer-sized delivery systems for contrast agents are being developed. A chylomicron-remnant-like vehicle of approximately 90 nm containing polyiodinated triglyceride analogs in a neutral lipid core has been developed as a hepatocyte-selective contrast agent for computed tomography in animals [31]. A paramagnetic liquid perfluorocarbon nanoparticle of approximately 250 nm to which an anti-$\alpha_V\beta_3$ antibody has been conjugated is being developed for MRI to assess angiogenesis and atherosclerosis [32,33]. However,

none of these are tumor targeting or currently applicable for cancer. However, given, as shown in Figure 1, that our nanocomplex can target metastatic disease it is anticipated that use of the nanocomplexed Magnevist® would also enhance detection sensitivity for metastases. The results shown here are with primary tumors. Studies are currently under way to compare the sensitivity of detection between free Magnevist® and the TfRscFv–Lip–Mag complex in metastases.

Using SEM and SPM we have also shown that the TfRscFv–Lip complex maintains its nanometer size when Magnevist® is encapsulated (particles of approximately 100–200 nm are shown in Figures 6 and 7). We have also demonstrated that the structural and mechanical properties of liposomes containing a payload are sufficiently different from those without one for it to be possible to confirm that Magnevist® is indeed encapsulated with the liposome. This was further confirmed by MFM imaging of the complex.

A tentative explanation for the internal structure of (Lip+Mag) is that the slight bulge in the SPM topographic image, represents a liposome-confined phase separation, that is, formation of a dense Magnevist–lipid toroidal distribution around the periphery of the particle with a preferential aqueous phase at the particle's center. This response is probably attributable to several important factors: First, the properties of Magnevist solution are pH approximately 6.5–8, an osmolality of 1,960, and viscosity of 4.9 at 20°C according to the manufacturer. A plausible chemical basis for this separation of the solution noted in the Magnevist data sheet: The meglumine salts dissociate completely from the complex, so changes in the local osmotic conditions. Coupled with the charge interaction of the gadolinium complex and cationic lipid, these interactions may provide a strong driving force for a hypertonic phase separation within the liposome. The charge distribution between the cationic lipid and Magnevist solution is effective at stabilizing the liposome and at providing structural support in solution and apparently in the bloodstream. This enhanced structural support is an important benefit for our studies because it enables most particles to remain intact during the film-drying process, in contrast to the extensive decomposition observed with the liposome-only solutions.

Therefore, we have been able to successfully encapsulate an MR contrast agent in our tumor-targeted nanodelivery system. The image enhancement demonstrated by the complex over conventionally delivered Magnevist® indicates the potential of this system to improve early detection of cancer via MRI.

Acknowledgments

We thank Ms. Brianna Kalk, Ms. Angelique Forrester, and Mr. Luis Torres for assistance in preparation of this manuscript, as well as the LCCC Animal Research Resource and Tissue Culture Shared Resource Facilities for their assistance in these studies. This work was supported in part by grants from NCI (CA103579-01) and SynerGene Therapeutics Inc (to K. F. P.) and from NFCR (to E. H. C.).

References

[1] Gillies RJ, Bhujwalla ZM, Evelhoch J, Garwood M, Neeman M, Robinson SP, Sotak CH, Van Der SB (2000). Applications of magnetic resonance in model systems: Tumor biology and physiology. *Neoplasia.* **2:**139–151.

[2] Degani H, Chetrit-Dadiani M, Bogin L, Furman-Haran E (2003). Magnetic resonance imaging of tumor vasculature. *Thromb Haemost.* **89:**25–33.

[3] Xu L, Pirollo K, Tang W, Rait A, Chang EH (1999). Transferrin–liposome-mediated systemic p53 gene therapy in combination with radiation results in regression of human head and neck cancer xenografts. *Hum Gene Ther.* **10:**2941–2952.

[4] Xu L, Pirollo K, Chang EH, Murray A (1999). Systemic p53 gene therapy in combination with radiation results in human tumor regression. *Tumor Targeting* **4:**92–104.

[5] Xu L, Tang WH, Huang CC, Alexander W, Xiang LM, Pirollo KF, Rait A, Chang EH (2001). Systemic p53 gene therapy of cancer with immunolipoplexes targeted by anti-transferrin receptor scFv. *Mol Med.* **7:**723–734.

[6] Xu L, Huang C-C, Huang W-Q, Tang W-H, Rait A, Yin Y, Cruz I, Xiang L-M, Pirollo K, Chang EH (2002). Systemic tumor-targeted gene delivery by anti-transferrin receptor scFv-immunoliposomes. *Mol Cancer Ther.* **1:**337–346.

[7] Rait A, Pirollo KF, Xiang LM, Ulick D, Chang EH (2002). Tumor-targeting, systemically delivered antisense HER-2 chemosensitizes human breast cancer xenografts irrespective of HER-2 levels. *Mol Med.* **8:**476–487.

[8] Rait A, Pirollo KF, Ulick D, Cullen K, Chang EH (2003). HER-2-targeted antisense oligonucleotides result in sensitization of head and neck cancer cells to chemotherapeutic agents. *Ann N Y Acad Sci.* **1002:**1–12.

[9] Cristiano RJ, Curiel DT (1996). Strategies to accomplish gene delivery via the receptor-mediated endocytosis pathway. *Cancer Gene Ther.* **3:**49–57.

[10] Cheng PW (1996). Receptor ligand-facilitated gene transfer: Enhancement of liposome-mediated gene transfer and expression by transferrin. *Hum Gene Ther.* **7:**275–282.

[11] Keer HN, Kozlowski JM, Tsai YC, Lee C, McEwan RN, Grayhack JT (1990). Elevated transferrin receptor content in human prostate cancer cell lines assessed in vitro and in vivo. *J Urol.* **143:** 381–385.

[12] Rossi MC, Zetter BR (1992). Selective stimulation of prostatic carcinoma cell proliferation by transferrin. *Proc Natl Acad Sci USA.* **89:**6197–6201.

[13] Elliott RL, Elliott MC, Wang F, Head JF (1993). Breast carcinoma and the role of iron metabolism. A cytochemical, tissue culture, and ultrastructural study. *Ann N Y Acad Sci.* **698:**159–166.

[14] Thorstensen K, Romslo I (1993). The transferrin receptor: Its diagnostic value and its potential as therapeutic target. *Scand J Clin Lab Invest Suppl.* **215:**113–120.

[15] Miyamoto T, Tanaka N, Eishi Y, Amagasa T (1994). Transferrin receptor in oral tumors. *Int J Oral Maxillofac Surg.* **23:**430–433.

[16] Ponka P, Lok CN (1999). The transferrin receptor: Role in health and disease. *Int J Biochem Cell Biol.* **31:**1111–1137.

[17] Haynes BF, Hemler M, Cotner T, Mann DL, Eisenbarth GS, Strominger JL, Fauci AS (1981). Characterization of a monoclonal antibody (5E9) that defines a human cell surface antigen of cell activation. *J Immunol.* **127:**347–351.

[18] Batra JK, Fitzgerald DJ, Chaudhary VK, Pastan I (1991). Single-chain immunotoxins directed at the human transferrin receptor containing *Pseudomonas* exotoxin A or diphtheria toxin: Anti-TFR(Fv)-PE40 and DT388-anti-TFR(Fv). *Mol Cell Biol.* **11:**2200–2205.

[19] Jain RK, Baxter LT (1988). Mechanisms of heterogenous distribution of monoclonal antibodies and other macro-molecules in tumors: Significance of elevated interstitial pressure. *Cancer Res.* **48:**7022–7032.

[20] Wolfert MA, Schacht EH, Toncheva V, Ulbrich K, Nazarova O, Seymour LW (1996). Characterization of vectors for gene therapy formed by self-assembly of DNA with synthetic block co-polymers. *Hum Gene Ther.* **7:**2123–2133.

[21] Dunlap DD, Maggi A, Soria MR, Monaco L (1997). Nanoscopic structure of DNA condensed for gene delivery. *Nucleic Acids Res.* **25:**3095–3101.

[22] Kawaura C, Noguchi A, Furuno T, Nakanishi M (1998). Atomic force microscopy for studying gene transfection mediated by cationic liposomes with a cationic cholesterol derivative. *FEBS Lett.* **421:**69–72.

[23] Choi YH, Liu F, Choi JS, Kim SW, Park JS (1999). Characterization of a targeted gene carrier, lactose–polyethylene glycol-grafted poly-L-lysine and its complex with plasmid DNA. *Hum Gene Ther* **10:**2657–2665.

[24] Diebel CE, Proksch R, Green CR, Neilson P, Walker MM (2000). Magnetite defines a vertebrate magnetoreceptor. *Nature.* **406:** 299–302.

[25] Rasa M, Kuipers BWM, Philipse AP (2002). Atomic force microscopy and magnetic force microscopy study of model colloids. *J Colloid Interface Sci.* **250:**303–315.

[26] Yu W, Pirollo KF, Yu B, Rait A, Xiang L, Huang W, Zhou Q, Ertem G, Chang EH (2004). Enhanced transfection efficiency of a systemically delivered tumor-targeting immunolipoplex by inclusion of a pH-sensitive histidylated oligolysine peptide. *Nucleic Acids Res.* **5**.

[27] Alisauskus R, Wong GY, Gold DV (1995). Initial studies of monoclonal antibody PAM4 targeting to xenografted orthotopic pancreatic cancer. *Cancer Res.* **55:**5743s–5748s.

[28] Foo JJ, Chan V, Liu KK (2003). Contact deformation of liposome in the presence of osmosis. *Ann Biomed Eng.* **31:**1279–1286.

[29] Xu L, Frederick P, Pirollo K, Tang W, Rait A, Xiang L, Huang W-Q, Chang EH (2002). Self-assembly of a virus-mimicking nanostructure system for efficient tumor-targeted gene delivery. *Hum Gene Ther.* **13:**469–481.

[30] Freedman M, Sarcone A, Pirollo KF, Lin C, Chang EH (2001). Ultrasound images of implanted tumors in nude mice using Sono-CT® correlated with MRI appearance. *SPIE Medical Imaging: Physiology and Function from Multidimensional Images.* **4321:**163–167.

[31] Wisner ER, Weichert JP, Longino MA, Counsell RE, Weisbrode SE (2002). A surface-modified chylomicron remnant-like emulsion for percutaneous computed tomography lymphography: Synthesis and preliminary imaging findings. *Invest Radiol.* **37:** 232–239.

[32] Winter PM, Morawski AM, Caruthers SD, Fuhrhop RW, Zhang H, Williams TA, Allen JS, Lacy EK, Robertson JD, Lanza GM, Wickline SA (2003). Molecular imaging of angiogenesis in early-stage atherosclerosis with alpha(v)beta3-integrin-targeted nanoparticles. *Circulation.* **108:**2270–2274.

[33] Morawski AM, Winter PM, Crowder KC, Caruthers SD, Fuhrhop RW, Scott MJ, Robertson JD, Abendschein DR, Lanza GM, Wickline SA (2004). Targeted nanoparticles for quantitative imaging of sparse molecular epitopes with MRI. *Magn Reson Med.* **51:**480–486.

Dual Probe with Fluorescent and Magnetic Properties for Imaging Solid Tumor Xenografts

Liang Shan[1], Songping Wang[1], Rajagopalan Sridhar[2], Zaver M. Bhujwalla[3], Paul C. Wang[1]

[1]Department of Radiology, Howard University, Washington D.C.
[2]Department of Radiation Oncology, Howard University, Washington D.C.
[3]Department of Radiology, Johns Hopkins University School of Medicine, Baltimore MD.

Correspondence: Paul C. Wang, Ph.D.
Department of Radiology, Howard University
2041 Georgia Ave, N.W., Washington DC 20060
Tel: 202-865-3711, Fax: 202-865-3722, E-mail: pwang@howard.edu

Running title
A dual probe for MRI and optical imaging

Key words: Tumor, imaging, transferrin, liposome, contrast agent

Abbreviations: CA, contrast agent; FI, fluorescent intensity; Lip, liposome; NIR, near-infrared; Tf, transferrin; TfR, transferrin receptor

Abstract

A dual probe with fluorescent and magnetic reporter groups was constructed by linkage of the near-infrared (NIR) fluorescent transferrin conjugate on the surface of contrast agent-encapsulated cationic liposome (Lip-CA). This probe was used for MRI and optical imaging of MDA-MB-231-luc breast cancer cells grown as monolayers *in vitro* and as solid tumor xenografts in nude mice. Confocal microscopy, optical imaging and MRI showed a dramatic increase of *in vitro* cellular uptake of the fluorescent and magnetic reporter groups from the probe compared to the uptake of CA or Lip-CA alone. Pretreatment with Tf blocked uptake of the probe reporters indicating the importance of the Tf moiety for targeting the probe to tumor cells. Intravenous administration of the dual probe to nude mice significantly enhanced the tumor contrast in MRI and preferential accumulation of the fluorescent signal was clearly seen in NIR-based optical images. More interestingly, the contrast enhancement in MRI showed a heterogeneous pattern within tumors, which reflected the tumor morphological heterogeneity. These results indicate that the newly developed dual probe enhances the tumor image contrast and is superior to CA alone for identifying the tumor pathological features on the basis of MRI, but also lends itself to fluorescent imaging.

I. Introduction

Tumor imaging exploits the differences in physical properties between malignant and normal tissues. These differences are often insufficient for good contrast resolution (1). Imaging techniques that improve tumor detection, localization and evaluation of therapy and prognosis would be highly desirable (2, 3). Contrast-enhanced magnetic resonance imaging (MRI) is one of the best noninvasive methodologies available today in clinical medicine for assessing anatomy and function of tissues (4). High spatial resolution and high soft tissue contrast are desirable features of noninvasive MRI. However, due to intrinsically low sensitivity, high local concentration of contrast agents (CA) is required to generate detectable MR contrast. A large amount of CA has to be used due to the non-specific uptake by tumors and other tissues *in vivo*. In recent years, targeted CA delivery systems have been developing based on the concept that molecular imaging can increase the signal to noise ratio by detecting the difference in 'molecular properties' between cancer and normal tissues (5-7). This should, in theory, allow for detection of smaller tumors. As one strategy, monoclonal antibodies or antibody fragments have been coupled with CA directly or linked with CA through liposome (Lip) carrier. High concentration of antibody-mediated CA such as Gd provides high T1 positive contrast *in vivo*, but insufficient direct linkage of Gd with antibody or the large molecular size of antibody-Lip-Gd particles may limit its use for imaging cell-surface receptors in solid tumors because of inefficient extravasation and very slow diffusion in the interstitial compartment (2, 8, 9). Furthermore, antibody immunogenicity, poor stability of the conjugates and potential change of the antibody binding ability due to changes in surface antigens are still problematic for *in vivo* application. A ligand with less toxic, high binding specificity for tumors, relative small size and without immunogenicity is required to target the CA to tumors.

Optical imaging offers several advantages over other imaging techniques. Among these are simplicity of the technique, high sensitivity and absence of ionizing radiation. There is a general increase in the development of techniques for *in vivo* evaluation of gene expression, monitoring of gene delivery and real-time intraoperative visualization of tumor margins and metastatic lesions to improve surgical outcome (10-12). Limited depth of light penetration and lack of tomographic information prevent *in vivo* efficiency of optical imaging. In order to overcome the limitations of various imaging modalities, multimodal probes have been developed for detection using multiple imaging devices (13-15).

Transferrin receptor (TfR) is a cell-surface internalizing receptor responsible for almost all iron sequestration in mammalian cells. Overexpression of TfR is reported on human cancers from various tissues including breast and is of great value in grading tumors and determining prognosis (16). TfR has been successfully applied as a molecular target to direct therapeutic agents to tumor cells (17). Transferrin (Tf), the TfR ligand, is a monomeric glycoprotein that binds Fe^{3+} atoms for delivery to vertebrate cells through receptor-mediated endocytosis. Fluorescently labeled Tf has greatly aided the investigation of endocytosis *in vitro*. *In vivo* use of the physiological serum protein Tf is less likely to cause adverse reactions. Indeed, Tf has been successfully used in targeted gene therapy (18, 19). We hypothesized that near-infrared dye (NIR) labeled Tf (Tf^{NIR}) would be an ideal ligand and

would selectively increase the cellular uptake of MRI and optical reporters *in vivo*, resulting in contrast-enhanced MRI and NIR-based optical detection. Herein, we developed a Tf- and Lip-mediated dual molecular probe with both fluorescent and magnetic reporter groups. The Tf^{NIR} was linked on the surface of Lip, whereas the MRI CA (Magnevist) was encapsulated within the Lip. These components conjugated together and formed uniform vesicles with less than 100 nm in diameter. *In vitro* analysis demonstrated that the probe dramatically improved the uptake of CA and NIR dye in culture cells through both receptor- and Lip-mediated endocytosis. *In vivo*, the probe significantly enhanced the magnetic resonance signals from the tumors and was superior to the CA alone for identifying the tumor morphology and infrastructure. Simultaneously a significant preferential accumulation of fluorescent signal by the tumors was clearly detectable in Tf^{NIR}-based optical imaging.

II. Materials and Methods

Materials

Cationic lipids including 1,2-dioleoyl-sn-glycero-3-phosphoethanolamine (DOPE), 1,2-dioleoyl-3-trimethylammonium-propane (DOTAP) and fluorescent lipid DOPE-N-(7-nitro-2-1,3-benzoxadiazol-4-yl) (NBD-DOPE) were purchased from Avanti Polar Lipids (Alabaster, AL). They were premixed and dissolved in chloroform in a formula of DOTAP:DOPE (1:1 w/w) (Lip) or in a fluorescent formula of DOTAP:DOPE + 0.1% NBD-DOPE (Lip^{NBD}). The CA Magnevist was obtained from Berlex Laboratories (Wayne, NJ). Fluorescent alexa fluor® 680 conjugate of human transferrin (Tf^{NIR}), SelectFX nuclear labeling kit, Alexa fluor 680 fluorophore and enzyme-free PBS-based cell dissociation solution were all purchased from Invitrogen (Carlsbad, CA). Holo-transferrin without fluorescent conjugate (Tf) and MicroSpin G-50 columns was obtained from Sigma (St. Louis, MO) and Amersham Biosciences (Piscataway, NJ), respectively. The SPI-Pore polycarbonate membrane filter and filter holder were from Structure Probe Inc (West Chester, PA).

Preparation of the molecular dual probe: Tf^{NIR}-Lip^{NBD}-CA complex

The Tf^{NIR}-Lip^{NBD}-CA complex was constructed using Tf^{NIR}, cationic Lip^{NBD} and Magnevist. Pre-mixed Lip^{NBD} in chloroform (3.607 μl) was dried under a nitrogen stream and hydrated by adding 50 μl pure water containing 12 μl Magnevist. The hydrated Lip^{NBD}-CA mixture was homogenized using a vortex generator and incubated for 10 minutes (min). The volume of the mixture was adjusted to 175 μl with pure water. The mixture was then sequentially down-sized by sonication (80-90 W, 10 min) in a water bath and by repeatedly passing through polycarbonate filters with decreasing pore diameter 0.2/0.1 μm. Following that, 25 μl of Tf^{NIR} (5 mg/ml) were mixed and incubated for at least 10 min. Gel-filtration through Sephadex G-50 column was used to remove un-encapsulated CA and free Tf^{NIR}. Freshly prepared probe was used in all analysis. The final volume was 200 μl and Lip:Tf:Magnevist composition was 10:12.5:0.56 (nmol/μg/mg). To monitor different components of the probe, non-fluorescent Tf and Lip were used instead of fluorescent Tf^{NIR} and Lip^{NBD} in some experiments.

Cell culture and animal model establishment

TfR-expressing MDA-MB-231-luc breast cancer cell line (Xenogen, Alameda, CA) was used to test the efficiency of the probe *in vitro* and *in vivo*. This cell line has been transfected with luciferase gene and expresses high level of luciferase. Cells were routinely maintained in DMEM/F-12 medium supplemented with 10% heat inactivated fetal bovine serum (FBS) and 50 μg/ml each of penicillin, streptomycin and neomycin (Invitrogen). The solid tumor xenograft model was developed by subcutaneous injection of $1x10^7$ subconfluent cells in 100 μl DPBS in the lower back of female athymic nude mice (8-10 weeks old, Harlan, Indianapolis, IN). The probe was evaluated in a total of 10 nude mice bearing tumors from 0.4 to 1.2 cm in diameter.

Confocal Microscopy

Tumor cells were grown on 8-chamber glass slides. Twenty-four hours later, the cells at 40-50% confluence were incubated with 25 μl of one of the following probes in 150 μl medium without FBS and antibiotics. The probes included Tf^{NIR}-Lip^{NBD}-CA**,** Tf-Lip^{NBD}-dye and dye alone. In order to visualize the cellular uptake of probe reporters, NIR dye alexa fluor 680 fluorophore was used to replace the CA in the preparation of Tf-Lip^{NBD}-dye probe at a concentration of 2 μl in 200 μl total probe. Incubation was carried out for 5, 30, 60 and 120 min, separately. After PBS washing (3 times), cells were fixed using 10% neutralized formalin for 10 min and cell nuclei were conterstained using DAPI blue-fluorescence dye. Confocal images were acquired with a Zeiss LSM 510 Confocal Microscopy System using 633 nm excitation line and emission LP 650 filter for Tf^{NIR} and Alexa fluor 680 fluorophore (red), 488 nm excitation line and emission BP 505 – 550 filter for Lip^{NBD} (green), and 364 nm excitation line and emission BP 385 – 470 filter for DAPI (blue). Following sequential excitation, red, green and blue fluorescent images of the same cells were merged using the Zeiss AIM software for co-localization of the probe different reporters within cells.

In vitro MRI and optical imaging

To quantify the cellular uptake of probe reporters, cell pellet optical imaging and MRI were performed. For optical imaging, similar numbers of tumor cells were seeded on 10 cm culture dishes and for MRI, in 150 cm flasks. Cells grown to subconfluence were incubated with 200 μl probe (in 3 ml medium) for 10 cm dishes and 600 μl probes (in 10 ml medium) for 150 cm flasks. Differently labeled probes were used including Tf^{NIR}-Lip^{NBD}-CA**,** Tf-Lip^{NBD}-dye, Lip^{NBD}-dye, CA alone and dye alone. Incubation was carried out for 60 min. After PBS washing (3 times), cells were collected using enzyme-free cell dissociation solution and adjusted to the same number. Cells were pelleted in microcentrifuge tubes by centrifugation. The cell pellets were quantified for the fluorescent intensity (FI) using Xenogen IVIS 200 imaging system (Xenogen) with ex/em filters at 679/702 nm for Tf^{NIR} and Alexa fluor 680 fluorophore, and at 464/531 nm for Lip^{NBD} measurement. Statistical analysis (Student's two-tailed t-test) of the FI for cells with different treatments was performed using Microsoft Excel. In order to get enough cells for MRI, cell pellets were pooled from five replicates and MRI was acquired using Bruker 400 MHz NMR machine (Bruker-Biospin, Billerica, MA). Multi-slice multi-echo T1-weighted sequence was used for imaging and Fast Imaging with Steady State Procession Sequence (FISP-T1Fit) was used for T1 measurement.

The MR images were taken at the cross-section direction of the microcentrifuge tubes. The imaging parameters are described in the figure legends. The central slice image which was not influenced by the image distortion due to the susceptibility effect from the air-pellet boundary was used for signal intensity measurement. All analyses were performed using the Bruker image sequence analysis tools. The T1 measurement parameters were TE = 1.5 ms, TR = 3 ms, number of averages = 8, number of frames = 16, number of segments = 32, inversion delay = 49.2 ms and inversion repetition = 2572.3 ms. All experiments were repeated at least 3 times. The representative data are presented.

In vivo MRI and optical imaging

The animal was anesthetized using 2% isoflurane and positioned with the tumor at the center of coil. The physiological condition of animals was monitored using a respiratory gating device during the scanning. The tumor was scanned in the coronal direction using a Bruker 400 MHz, 89 mm vertical bore size NMR spectrometer. A multi-slice multi-echo T1-weighted sequence was used for imaging with a slice thickness of 1 mm. For each animal, a baseline image was first obtained; the tumors were then sequentially imaged at an interval of about 10 min until 3 h following i.v. administration of 200 µl of Tf^{NIR}-Lip^{NBD}-CA probe (containing 12 µl Magnevist) through the tail vein. For comparative study, the same animals were also imaged following i.v. administration of the same dosage of CA alone (12 µl Magnevist in 200 µl pure water). The interval period between the two MRI studies was at least 3 days in order to remove the influence of CA from the previous study. For optical imaging, the FI of tumors was monitored from 10 min to 3 or 5 days following i.v. administration of the probe using Xenogen IVIS 200 imaging system.

Pathological analysis

After imaging, the mice were autopsied and the tumors were sampled and fixed in 10% neutral buffered formalin. Tumors were sectioned in the same direction as MR images. Hematoxylin-eosin (HE) staining was used for pathological examination. A comparison was performed between the pathological findings of tumors and the enhancement pattern in MRI.

III. RESULTS

Visualization of Tf- and Lip-mediated cellular uptake

For confocal microscopic observation of the cellular uptake of the probe reporters, cells were incubated with the probe Tf-Lip^{NBD}-dye or dye alone from 5 min to 2 h. Here, the probe was constructed using unlabeled Tf and NIR fluorescent dye instead of CA in order to visualize the uptake of encapsulated reagents within Lip. Figure 1 shows representative microscopic images. Both Lip^{NBD} (green) and fluorescent dye (red) were observed to be present in the cell cytoplasm as early as 5 min after incubation with the probe and their FI within the cytoplasm increased gradually, reaching a maximum at about 1 h incubation (Fig. 1A-C). Interestingly, the Lip^{NBD} and dye accumulated again, forming multiple endosomes. These endosomes were mainly located at the peripheral area of the cytoplasm and became more evident at 2 h incubation (Fig. 1D-F), suggesting receptor-mediated endocytosis, and

release or degradation of the probe reporters through introduction of lysosomal enzymes. Cellular uptake of the dye was not evident in the cells incubated with dye alone.

To visualize whether the Tf and Lip were co-internalized, confocal microscopy and optical imaging were performed for cells incubated with Tf^{NIR}-Lip^{NBD}-CA, Lip^{NBD}-CA or CA alone. Similarly, from 5 min incubation, the Tf^{NIR} (Fig. 2A) and Lip^{NBD} (Fig. 2B) were already co-localized within cell cytoplasm (Fig. 2C). Optical imaging of the cell pellets further confirmed the uptake of the probe in tumor cells. To avoid membrane damage and probe leakage from cells, enzyme-free PBS-based cell dissociation solution was used instead of trypsin for cell dissociation from culture dishes. As shown in Fig. 2D, only cells incubated with Tf^{NIR}-Lip^{NBD}-CA showed strong fluorescent signal of Tf^{NIR}. Both cells incubated with Tf^{NIR}-Lip^{NBD}-CA , and cells incubated with Lip^{NBD}-CA showed strong fluorescent signal of Lip^{NBD}. Neither Tf^{NIR} nor Lip^{NBD} signal was detectable in cells incubated with CA alone.

We further evaluated whether the CA encapsulated within the probe was internalized into tumor cells using MRI of the cell pellets. A representative MR image of the cell pellets obtained from cells incubated with Tf^{NIR}-Lip^{NBD}-CA, Lip^{NBD}-CA or CA alone is shown in Figure 2F. The corresponding signal intensity and T1 relaxation time are shown in table 1. Cells incubated with the probe Tf^{NIR}-Lip^{NBD}-CA or Lip^{NBD}-CA showed a much greater positive contrast and T1 shortening than the cells incubated with CA alone ($P < 0.05$). The cells incubated with Tf^{NIR}-Lip^{NBD}-CA also showed higher signal intensity than the cells incubated with Lip^{NBD}-CA. These results highly indicate the importance and specificity of Tf moiety for targeting the probe internalization into tumor cells *in vitro*.

Quantification of Tf- and Lip-mediated cellular uptake

To evaluate the efficiency of Tf- and Lip-mediated cellular uptake, the FI of the Lip^{NBD} and NIR dye within the tumor cells was quantified following 1 h incubation of the cells with probes. The FI of NIR dye in the cells incubated with Tf-Lip^{NBD}-dye and with Lip^{NBD}-dye was more than 200-fold higher than that in the cells with dye alone (table 2). Cells incubated with dye alone showed similar level of FI to cells without probe and dye exposure (autofluorescence background). Approximate 1.5-fold higher FI of the intracellular NIR dye was also obtained in cells incubated with Tf-Lip^{NBD}-dye than in cells incubated with Lip^{NBD}-dye. Similarly, 2-fold higher FI of Lip^{NBD} was detected in cells incubated with Tf-Lip^{NBD}-dye or Lip^{NBD}-dye than in cells incubated with NIR dye alone (autofluorescent background) (table 2). The FI of Lip^{NBD} was 1.3-fold higher in cells incubated with Tf-Lip^{NBD}-dye than in cells incubated with Lip^{NBD}-dye. Student's t-test (2-tailed) between cells incubated with probe and with dye alone for both intracellular Lip^{NBD} and NIR dye intensity were both significant ($P<0.05$). The FI in cells incubated with Tf-Lip^{NBD}-dye and in cells incubated with Lip^{NBD}-dye were also significantly different ($P<0.05$) for both intracellular Lip^{NBD} and NIR dye uptake.

To further test the specificity of Tf-mediated cellular uptake, cells were first pre-treated for 1 h with unlabeled Tf before incubation with the probes. The amount of Tf was 3-fold (375 μg/dish) higher than that used in the probe (125 μg/dish). Following incubation with the probe Tf-Lip^{NBD}-dye, the FI of the NIR dye in cells with and without Tf pretreatment was $2.45x10^9$ and $3.42x10^9$ p/s/cm^2/sr, respectively (table 3). The FI of the Lip^{NBD} in cells with and without Tf pretreatment was $2.57x10^7$ and $3.45x10^7$ p/s/cm^2/sr, respectively. Calculation

based on the control cells incubated with Lip^{NBD}-dye revealed a blockage of 65.6% of the dye uptake and 70.97% of the Lip^{NBD} uptake by Tf pretreatment. These results indicate that the probe reporter uptake *in vitro* was mediated by both Tf and cationic Lip. Tf and Lip have an apparent synergistic effect on the cellular uptake of the probe reporters.

Probe-mediated signal enhancement of the tumors in vivo

Signal enhancement was evaluated in 10 athymic nude mice with solid tumor xenografts. The tumor size ranged from 0.4 to 1.2 cm in diameter. In order to compare the signal enhancement mediated by the probe and mediated by the CA alone, same mice were used for the probe and CA alone studies sequentially with an interval of at least 3 days. Intravenous administration of the probe Tf^{NIR}-Lip^{NBD}-CA significantly enhanced the tumor image contrast (Fig.3). The enhancement was observed as early as 10 min after administration and increased gradually, reaching the maximum at 90 min to 2 h. After that, gradual decrease of the signal enhancement was observed. Interestingly, the enhancement was greatly heterogeneous within the tumors (Fig. 3). The enhancement pattern became relatively consistent from 1 to 3 h. Some areas of the tumors were strongly enhanced initially and other areas were weakly enhanced. The signals from strongly enhanced region decreased much slower than the signals from region with weak enhancement. For small tumors, the enhancement was relatively uniform and the enhancement was usually observed beginning from peripheral area. Magnevist alone slightly enhanced the image contrast of tumors compared to the baseline images (Fig. 4). The maximum enhancement was observed usually at 30 to 60 min after administration. The image contrast enhancement started from peripheral area to the center of tumors and was relatively uniform within tumors irrespective of their sizes studied here. The signal enhancement decreased rapidly and returned to baseline within 3 h.

Detection and dynamic change of the fluorescent signal in tumors in vivo

To understand whether the probe was preferentially accumulated in tumors and whether the fluorescent signal was optically detectable *in vivo*, tumors were monitored using Tf^{NIR}-based optical imaging. Fluorescent signal was clearly detectable as early as 10 min and reached the maximum intensity at about 90 min to 2 h after i.v. injection of the probe Tf^{NIR}-Lip^{NBD}-CA (Fig.5). The FI was related to the tumor sizes and significant FI was still detectable after 2 days for larger tumors (usually > 0.8 cm in diameter). FI of smaller tumors became very weak at 24 h. The FI of Lip^{NBD} was too weak to be detectable by optical imaging *in vivo*, although clearly detected *ex vivo*. High autofluorescent background was another reason for the failure to detect Lip^{NBD} in tumors. Both *ex vivo* and *in vivo* optical imaging and MRI revealed a high fluorescence and CA signal in liver, gallbladder, kidney and bladder, suggesting that the probe was cleared mainly from kidney and liver. However, detailed analysis will be necessary for a complete analysis of *in vivo* pharmacokinetics of the dual probe.

Comparison between MRI signal enhancement and pathological findings

To understand the underlying mechanism of heterogeneous contrast enhancement within the tumors by the probe, a comparative analysis was performed between MRI signal enhancement and pathological findings (Fig. 6). Pathologically, the tumor cells in large

tumors with heterogeneous enhancement usually presented various stages of growth and necrosis. In some areas, the tumor cells were completely necrotized and became amorphous and liquefied. In some other regions, the tumor cells showed dying features such as condensed or broken nuclei or only shadow cells left. The mostly enhanced regions of the tumors in MR images represented the more actively proliferating tumor cells in pathology versus the weakly enhanced areas, the less active or dying cells. The completely necrotized region showed least enhancement. The heterogeneous signal enhancement by the probe was well correlated with the *in vivo* morphological features of the tumors.

IV. Discussion

The human Tf-targeted cationic liposome-DNA complex has been used for efficient gene transfer in animal models recently. The formulation for optimal transfection of cancer cells has been optimized as DNA:Lipid:Tf ratio of 1 μg:10 nmol:12.5 μg with liposome composition of DOTAP:DOPE (1:1, w/w). This complex of Tf-Lip-DNA demonstrates a highly compact structure that resembles a virus particle with a dense core enveloped by a membrane coated with Tf molecules spiking the surface (20, 21). Successful gene delivery using Tf-targeted cationic liposome is based on the facts that TfR is over-expressed in most malignant tumors and Tf-TfR-mediated endocytosis is highly efficient. Furthermore, cationic liposome shows many advantages such as great encapsulating capacity, much less immunogenicity and toxicity, and dramatically increased transfection efficiency through linkage with ligands (22). These characteristics of this system also fulfill the criteria as an ideal system for molecular imaging *in vivo*. Using the advantages of this system, we developed the probe with both NIR fluorescence and MRI reporters, which is suitable for both optical and NMR imaging. Use of NIR fluorescence molecule minimizes the autofluorescence interference from healthy tissue and allows the visualization of tissues millimeters in depth because of efficient penetration of photons in near-infrared range (11, 12). To encapsulate the CA, we directly hydrated the dried Lip films with less diluted CA solution and down-sized the Lip-CA complex by sonication and repeated passing through the membrane before linkage with Tf. The Lip:Tf ratio (10:12.5) used in the probe was optimized as reported previously (20-24). The dosage of Magnevist was 0.2 mmol/kg, corresponding to 30 gram mouse as recommended by the manufacturer. For this amount of Magnevist (even 3-fold more), almost all of the Magnevist was found to be encapsulated within the Lip through gel filtration and fluorescence study. Our previous study also confirmed Magnevist encapsulation within Lip using scanning electron microscopy and scanning probe microscopy (25). The Tf, cationic Lip and gadolinium complex were coupled through charge interaction, which makes the preparation of the probe simple enough to be freshly prepared before use. A concern for Lip carrier as in the gene delivery is its size. It has been reported that linkage with Tf condenses the Lip-DNA complex with a uniform size of 50-90 nm (20, 23). After sonication of the probe, we found that repeated passing through 200 and 100 nm polycarbonate membranes only resulted in a loss of less than 10% of the probe and majority of the probe particles were within 100 nm in size based on the fluorescence Lip quantification. Transportation of the probe across tumor vessels occurs via open gaps, vesicular vacuoles

and/or fenestrations. A characteristic pore cutoff size is measured ranging from 200 nm to 1.2 μm in tumors (26). Another analysis points out that the pore cutoff size is around 400 nm based on *in vivo* fluorescence microscopy studies of the transportation of sterically stabilized Lip into solid tumors (27). Therefore, size of our probe should not be a limitation to transport from tumor vasculature into tumor cells.

We first evaluated the probe-mediated uptake efficiency of the reporters *in vitro*. To visualize and quantify the efficiency, the components of the probe were differentially labeled. On confocal microscopy, Tf^{NIR}, Lip^{NBD} and the encapsulated NIR dye were clearly co-distributed within the cytoplasm of tumor cells. They accumulated and formed endosomes again in the peripheral area of the cytoplasm. In the Tf-Lip-mediated plasmid DNA transfection, similar endosome formation has been reported by Lee SM and Kim JS (28). They also found a nuclear localization of the Tf-Lip. In our system, no nuclear signal of the probe was observed. Quantitative analysis using optical imaging further confirmed the finding of confocal microscopy. The cellular uptake was mediated by both Tf and Lip. Blockage of the TfR with Tf led to significantly decreased uptake. The possibility of nonspecific binding to free NIR dye was excluded because no fluorescent signal of the dye was detected in cells incubated with dye alone. Lip-mediated uptake is already widely used for *in vitro* gene transfection and *in vivo* gene delivery (22). Therefore, higher cellular uptake of the Lip and dye in cells incubated with Lip^{NBD}-dye than in cells incubated with dye alone is not surprising. Importantly, Tf and Lip showed a synergistic effect on the cell uptake based on our quantitative and blocking analysis. MRI of the cell pellets revealed a similar finding that CA is internalized and the internalization is mediated by both Tf and Lip. The apparent synergistic effect may be explained by a 3-step mechanism. The important first step is the specific binding of Tf with TfR on the cell surface followed by the interaction of cationic Lip with anionic cell membrane and finally is the receptor- and Lip-membrane fusion-mediated endocytosis (29).

Consistent with our *in vitro* findings, specific targeting of the probe *in vivo* was demonstrated by both optical imaging and MRI. A preferential accumulation of the fluorescent signal in tumors and a significant signal enhancement are clearly detected with dual probe over the CA alone. Time course study revealed a high consistency among confocal images, optical fluorescence and MRI contrast enhancement. The maximum signal enhancement and FI in tumors are detected around 90 min and both achieved a plateau between 1 to 3 h after i.v. injection. Whereas the maximal enhancement is achieved at about 45 min following administration of CA alone and the enhancement reduces to baseline within 3 h. The signal enhancement achieved by the probe is much stronger than that achieved by the CA alone. These results are consistent with the finding in gene therapy using Tf-mediated Lip system that high gene transfection efficiency was observed within tumors (23, 24). More interestingly, heterogeneous enhancement in MR images is evident in large tumors, which is correlated with the pathological findings. Within the range of tumor sizes in the present study, CA alone could enhance the image contrast, but the enhancement was weak and relatively uniform. Heterogeneous enhancement may be potentially valuable. It makes it possible to interpret the pathological features based on specifically enhanced MRI. More information could be provided to the clinician without further invasive procedure of biopsy (3, 30). Quantitative study may be necessary to evaluate the relationship between the expression

levels of specific molecules such as Tf and the enhancement levels in MRI. Of course, we can not rule out the non-specific accumulation of the probe in tumors such as Lip alone-mediated endocytosis and non-specific uptake of CA and accumulation within the interstitial space and immature tumor vessels. An example for the non-specificity is the enhancement in the necrotic area, which may be due to the leakage of the probe, although it is very weak. Fortunately, it seems that presence of non-specific enhancement does not interfere with the potentiality to interpret the tumor pathology by enhanced MRI. Clear detection by optical imaging gives us another interesting clue that our probe can be not only used for optical detection of tumors, but also may be possible to quantify the tumors such as the expression level of Tf and tumor cell growth. These parameters are of great value in predicting the prognosis and treatment selection. This goal can be achieved using the advantage of quantitative ability of optical imaging. However, limited penetration of fluorescence is still a problem, particularly for deep organ tumors. Clearly, use of multi-modality reporter constructs can overcome many of the shortcomings of each modality alone (14, 15).

In conclusion, we developed a novel nano-sized molecular probe with both optical and MRI reporters. *In vitro* and *in vivo* analysis confirmed the probe specificity, internalizing efficiency and sufficiency for multi-modality detection. In MRI, the probe significantly enhances the tumor contrast so that it can increase the sensitivity to detect small tumors. Tumor enhancement pattern could help to evaluate the pathological features of tumors *in vivo*, which provides more information for clinician. Preferential accumulation of the probe NIR fluorescence makes the tumor detectable using NIR-based optical imaging. Furthermore it provides the possibility to quantify the specific biomarkers expressed in tumors, which will be helpful to determine the patient's outcome and treatment selection.

Acknowledgments:

We thank Dr. Elizabeth G. Snyderwine and Dr. Minshu Yu (Laboratory of Experimental Carcinogenesis, NCI, NIH) for their scientific advice. We are grateful to Stephen M. Wincovitch and Susan H. Garfield (CCR Confocal Microscopy Core Facility, NCI, NIH) for help and consultation with confocal microscopy. This study was supported by the following grants: NIH/NCRR/RCMI 2G12RR003048, USAMRMC W81XWH-05-1-0291 and NIH 5U54CA091431.

References:

[1] Pautler RG (2004). Mouse MRI: concepts and applications in physiology. *Physiol*. **19**:168-175.

[2] Artemov D (2003). Molecular magnetic resonance imaging with targeted contrast agent. *J Cell Biochem*. **90**: 518-524.

[3] Massoud TF, Gambhir SS (2003). Molecular imaging in living subjects: seeing fundamental biological processes in a new light. *Gene Dev*. **17**:545-580.

[4] Persigehl T, Heindel W, Bremer C (2005). MR and optical approaches to molecular imaging. *Abdom Imaging*. **30**:342-354.

[5] Blasberg RG (2003). Molecular imaging and cancer. *Mol Cancer Ther*. **2**:335-345.

[6] Funovics MA, Kapeller B, Hoeller C, Su HS, Kunstfeld R, Puig S, Macfelda K (2004). MR imaging of the her2/neu and 9.2.27 tumor antigens using immunospecific contrast agents. *Magn Reson Imaging*. **22**:843-850.

[7] Basilion JP (2001). Current and future technologies for breast cancer imaging. *Breast Cancer Res*. **3**:14-16.

[8] Artemov D, Mori N, Okollie B, Bhujwalla ZM (2003). MR molecular imaging of HER-2/neu receptor in breast cancer cells using targeted iron oxide nanoparticles, *Magn Reson Med*. **49**:403-408.

[9] Mulder WJM, Strijkers GJ, Griffioen AW, van Bloois L, Molema G, Storm G, Koning GA, Nicolay K (2004). A liposomal system for contrast-enhanced magnetic resonance imaging of molecular targets. *Bioconjugate Chem*. **15**:799-806.

[10] Graves EE, Weissleder R, Ntziachristos V (2004). Fluorescence molecular imaging of small animal tumor models. *Curr Mol Med*. **4**:419-430.

[11] Ntziachristos V, Bremer C, Weissleder R (2003). Fluorescence imaging with near-infrared light: new technological advances that enable in vivo molecular imaging. *Eur Radiol*. **13**:195-208.

[12] Hoffman RM (2005). The multiple uses of fluorescent proteins to visualize cancer in vivo. *Nature* **5**:796-806.

[13] Schellenberger EA, Sosnovik D, Weissleder R, Josephson L (2004). Magneto/optical annexin V, a multimodal protein. *Bioconjugate Chem*. **15**:1062-1067.

[14] Blasberg RG (2003). In vivo molecular-genetic imaging: multi-modality nuclear and optical combinations. *Nucl Med Biol*. **30**:879-888.

[15] Veiseh O, Sun C, Gunn J, kohler N, Gabikian P, Lee D, Bhattarai N, Ellenbogen R, Sze R, Hallahan A, Olson J. Zhang M (2005). Optical and MRI multifunctional nanoprobe for targeting gliomas. *Nano Lett*. **5**:1003-1008.

[16] Jones DT, Trowbridge IS, Harris AL (2006). Effects of transferrin receptor blockade on cancer cell proliferation and hypoxia-inducible factor function and their differential regulation by ascorbate. *Cancer Res*. **66**:2749-2756.

[17] Hogemann-Savellano D, Bos E, Blondet C, Sato F, Abe T, Josephson L, Weissleder R, Gaudet J, Sgroi D, Peters PJ, Basilion JP (2003). The transferrin receptor: a potential molecular imaging marker for human cancer. *Neoplasia*. **5**:495-506.

[18] Xu L, Pirollo KF, Tang Wh, Rait A, Chang EH (1999). Transferrin-liposome-mediated systemic p53 gene therapy in combination with radiation results in regression of human head and neck cancer xenographs. *Hum Gene Ther*. **10**:2941-2952.
[19] Bellocq NC, Pun SH, Jensen GS, Davis ME (2003). Transferrin-containing, cyclodextrin polymer-based particles for tumor-targeted gene delivery. *Bioconjugate Chem*. **14**:1122-1132.
[20] Xu L, Frederik P, Pirollo KF, Tang W, Rait A, Xiang L, Huang W, Cruz I, Yin Y, Chang EH (2002). Self-assembly of a virus-mimicking nanostructure system for efficient tumor-targeted gene delivery. *Hum Gene Ther*. **13**:469-481.
[21] Kursa M, Walker GF, Roessler V, Ogris M, Roedl W, Kircheis R, Wagner E (2003). Novel shielded transferring-polyethylene glycol-polyethylenimine/DNA complexes for systemic tumor-targeted gene transfer. *Bioconjugate Chem*. **14**:222-231.
[22] Simoes S, Pires P, Duzgunes N, Pedroso de Lima M (1999). Cationic liposomes as gene transfer vectors: Barriers to successful application in gene therapy. *Curr Opin Mol Theory*. **1**:147-157.
[23] Nakase M, Inui M, Okumura K, Kamei T, Nakamura S, Tagawa T (2005). p53 gene therapy of human osteosarcoma using a transferring-modified cationic liposome. *Mol Cancer Ther*. **4**:625-631.
[24] Pirollo KF, Xu L, Chang EH (2002). Non-viral gene delivery for p53. *Curr Opin Mol Ther*. **2**:168-175.
[25] Pirollo K, Dagata J, Wang P, Freedman M, Vladar A, Fricke S, Ileva L, Zhou Q, Chang EH (2006). A tumor-targeted nanodelivery system to improve early MRI detection of cancer. *Mol Imaging*. **5**:
[26] Hobbs SK, Monsky WL, Yuan F, Roberts WG, Griffith L, Torchilin VP, Jain RK (1998). Regulation of transport pathways in tumor vessels: role of tumor type and microenvironment. *Proc Natl Acad Sci USA*. **95**:4607-4612.
[27] Unezaki S, Maruyama K, Hosoda JI, Nagae I, Koyanagi Y, Nakata M, Ishida O, Iwatsuru M, Tsuchiya S (1996). Direct measurement of extravasation of poly-ethyleneglycol-coated liposomes into solid tumor tissue by in vivo fluorescence microscopy. *Int J Pharm*. **144**:11-17.
[28] Lee SM, Kim JS (2005). Intracellular trafficking of transferring-conjugated liposome/DNA complexes by confocal microscopy. *Arch Pharm Res*. **28**:93-99.
[29] Yin J, Lin AJ, Buckett PD, Wessling-Resnick M, Golan DE, Ealsh CT (2005). Single-cell FRET imaging of transferrin receptor trafficking dynamics by sfp-catalyzed, site-specific protein labeling. *Chem Biol*. **12**:999-1006.
[30] Mankoff D (2005). Imaging in breast cancer-breast cancer imaging revisited. *Breast Cancer Res*. **7**:276-278.

Table 1. Comparison between probe- and CA-mediated signal enhancement

	Tf^{NIR}-Lip^{NBD}-CA	Lip^{NBD}-CA	CA alone
Relative Intensity (10^5):	17.7±0.86	15.33±0.86	13.25±0.78
T1 relaxation time (ms):	366.7±17.1	374.3±17.3	408.1±13.8

$P < 0.05$ between probe and CA alone for both relative intensity and T1.

Table 2: Optical quantitation of probe-mediated cellular uptake of reporters

Reporters	Tf-Lip^{NBD}-dye	Lip^{NBD}-dye	dye alone
NIR dye (x 10^9)	6.88±0.59	4.99±0.51	0.23±0.006
Lip^{NBD} (x 10^7)	2.03±0.14	1.64±0.09	1.10±0.13

$P<0.05$ between probe and dye alone and also between Tf-Lip^{NBD}-dye and Lip^{NBD}-dye for both dye and Lip^{NBD} uptake. Quantitation is based on the fluorescence intensity (p/s/cm2/sr) of cell pellets.

Table 3: Blockage of Tf-mediated uptake of reporters by Tf pretreatment

Reporters	Tf-Lip^{NBD}-dye untreated	Tf-Lip^{NBD}-dye pre-treated	Lip^{NBD}-dye alone
NIR dye (x10^9)	3.42±0.17	2.45±0.21	1.94±0.20
Lip^{NBD} (x10^7)	3.45±0.29	2.57±0.21	2.21±0.16

$P<0.05$ between pre-treated and untreated cells for both dye and Lip^{NBD} uptake.

Quantitation is based on the fluorescence intensity (p/s/cm2/sr) of cell pellets.

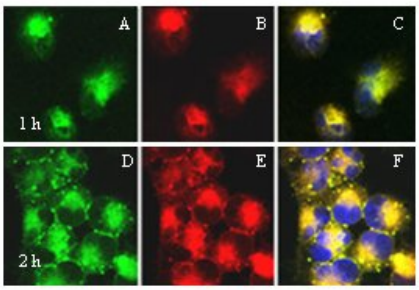

Figure 1. Confocal microscopic observation of cellular uptake of probe reporters. Cells were incubated with the probe Tf-LipNBD-dye for 5 min to 2 h. Panels A-C are representative images acquired at 1 h incubation time point, showing distribution and co-localization of LipNBD (A) and NIR dye (B) in the cytoplasm. Panels D-F are representative images acquired at 2 h incubation time point, showing multiple endosomes formed by Lip (D) and NIR dye (E), and co-localized in the peripheral area of the cytoplasm (F). Nuclei were counter-stained using DAPI.

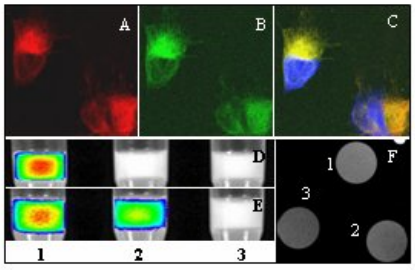

Figure 2. Confocal, optical and MRI detection of the reporters in cells incubated with the probe TfNIR-LipNBD-CA for 1 h. Panels A-C are representative confocal microscopic images, showing distribution and co-localization of TfNIR (A) and LipNBD (B) in cytoplasm. Panels D-E are optical images of the cell pellets. Strong fluorescent signal of Tf is detected in cells incubated with TfNIR-LipNBD-CA (D, lane 1), but not in cells incubated with LipNBD-CA or with CA alone (D, lane 2 and 3). Similarly, strongest signal of LipNBD is detected in cells incubated with TfNIR-LipNBD-CA (E, lane 1) and less in cells incubated with LipNBD-CA (E, lane 2), but not in cells incubated with CA alone (E, lane 3). Panel F shows the MR images of the cell pellets. A stronger signal enhancement and T1 shortening are obtained in cells incubated with TfNIR-LipNBD-CA and in cells incubated with LipNBD-CA (1 and 2) than in cells incubated with CA alone (3). The MR imaging parameters are TE = 11.416 ms, TR = 500 ms, number of averages = 4, field of view = 20 x 20 mm, matrix size = 256 x 128 and slice thickness = 2 mm.

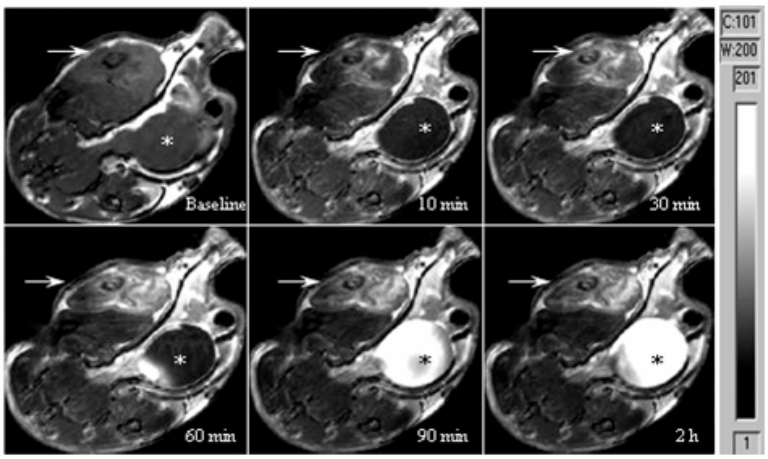

Figure 3. In vivo time course of tumor MRI after i.v. administration of the probe TfNIR-LipNBD-CA, showing gradually increased enhancement of the tumor signal (arrow) and heterogeneous enhancement pattern. Gradual accumulation of CA in the urinary bladder is evident (*). The MRI parameters are TE = 11.416 ms, TR = 800 ms, number of average = 4, field of view = 28 x 30 mm, matrix size = 256 x 192, and slice thickness = 1.0 mm.

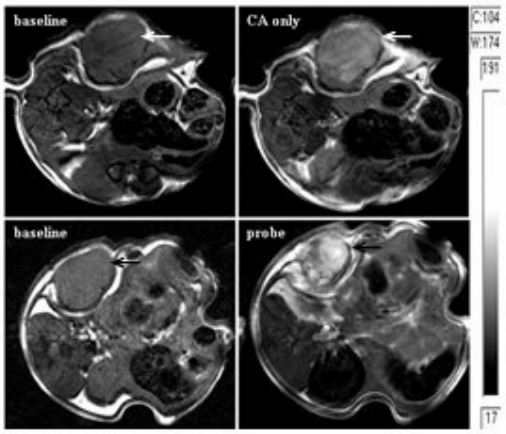

Figure 4. Comparison of the signal enhancement by CA alone (panels A-B) and by the probe TfNIR-LipNBD-CA (panels C-D). The MR images are from the same tumor with an interval of 72 h between studies with the probe and with CA alone. A stronger and heterogeneous signal enhancement is achieved with TfNIR-LipNBD-CA over CA alone. The MRI parameters are the same as for Fig. 3.

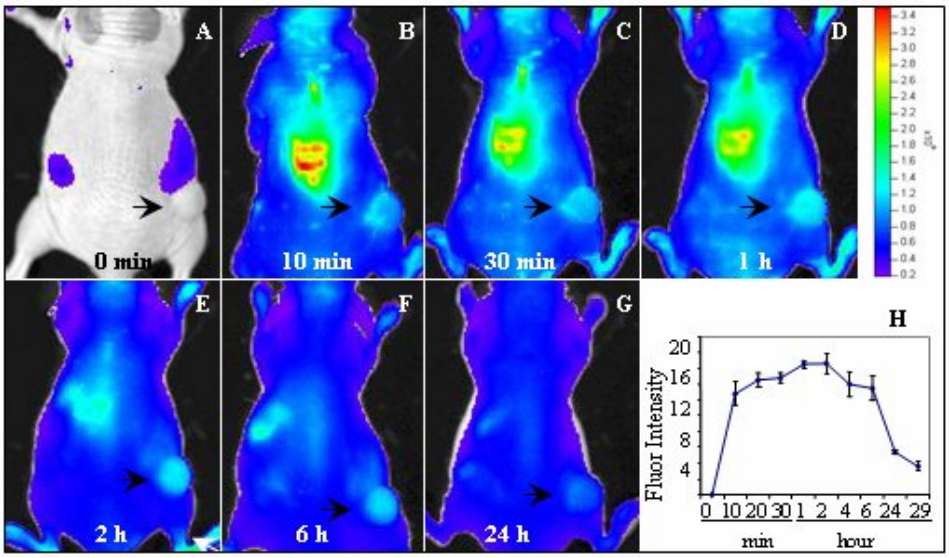

Figure 5. Optical imaging of the tumor after i.v. administration of Tf^{NIR}-Lip^{NED}-CA, showing preferential accumulation of fluorescent signal in tumors. The fluorescence signal was detectable as early as 10 min and reached a maximum at about 2 h and then deceased gradually (7H). The signal intensity is expressed as p/s/cm^2/sr.

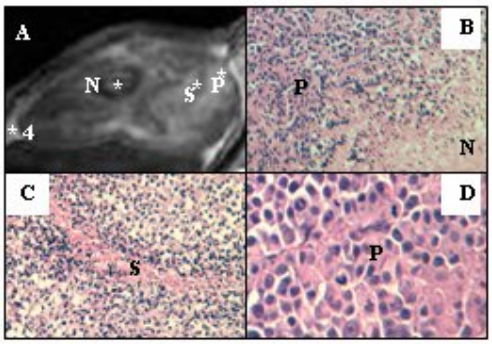

Figure 6. Correlation of MRI with pathological findings, showing high consistency between probe-mediated enhancement pattern in MRI and pathological findings (HE stain). Panel A is a representative MR image (same as Fig. 3) showing heterogeneous enhancement pattern. Panel B shows a region with high proliferation and necrosis (x 250). Panel C shows the stromal tissue (x 250) and panel D shows the proliferating tumor cells with high mitotic activity (x 400). P, proliferating cells; N, necrosis; S, stromal tissue; F, fat tissue.

NMR Instrumentation

Varian 4.7T

200 MHz

horizontal bore

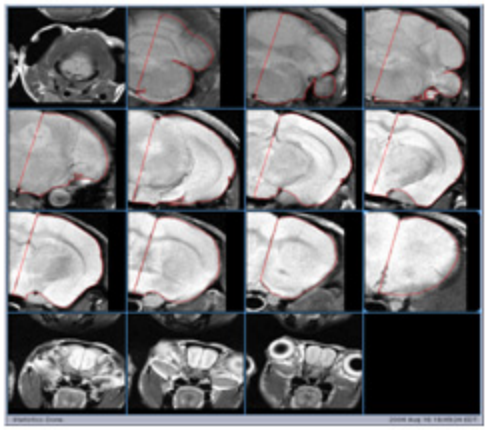

Bruker 9.4T

400 MHz

89 mm bore

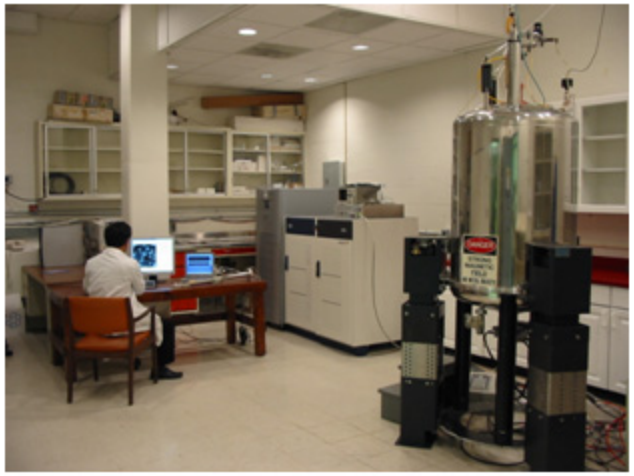

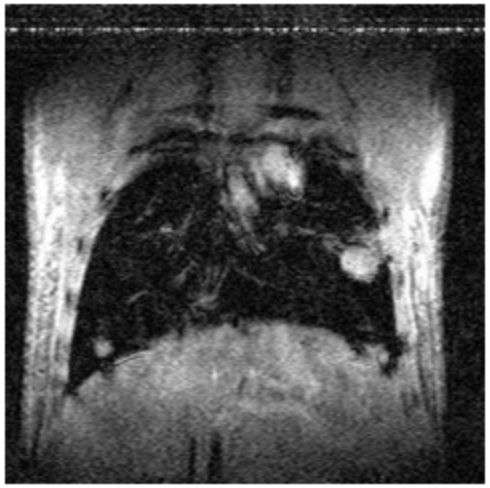

Optical Instrument

Xenogen IVIS 200